

Estimating Redshifts for Long Gamma-Ray Bursts

Limin Xiao and Bradley E. Schaefer

Physics and Astronomy, Louisiana State University, Baton Rouge, LA, 70803

Received _____; accepted _____

arXiv:0910.4945v1 [astro-ph.CO] 26 Oct 2009

ABSTRACT

The measurement of redshifts for Gamma-Ray Bursts (GRBs) is an important issue for the study of the high redshift universe and cosmology. We are constructing a program to estimate the redshifts for GRBs from the original *Swift* light curves and spectra, aiming to get redshifts for the Swift bursts *without* spectroscopic or photometric redshifts. We derive the luminosity indicators from the light curves and spectra of each burst, including the lag time between low and high photon energy light curves, the variability of the light curve, the peak energy of the spectrum, the number of peaks in the light curve, and the minimum rise time of the peaks. These luminosity indicators can each be related directly to the luminosity, and we combine their independent luminosities into one weighted average. Then with our combined luminosity value, the observed burst peak brightness, and the concordance redshift-distance relation, we can derive the redshift for each burst. In this paper, we test the accuracy of our method on 107 bursts with known spectroscopic redshift. The reduced χ^2 of our best redshifts (z_{best}) compared with known spectroscopic redshifts (z_{spec}) is 0.86, and the average value of $\log_{10}(z_{best}/z_{spec})$ is 0.01, with this indicating that our error bars are good and our estimates are not biased. The RMS scatter of $\log_{10}(z_{best}/z_{spec})$ is 0.26, with a comparison of 0.30 for RMS of $\log_{10}(z_{spec})$. We made a selection on bursts with relatively accurate redshift estimation. The RMS of $\log(z_{best}/z_{spec})$ decreases to 0.19, and the RMS scatter of $\log_{10}(z_{spec})$ for this subsample is 0.28. For *Swift* bursts measured over a relatively narrow energy band, the uncertainty in determining the peak energy is one of the main restrictions on our accuracy. Although the accuracy of our z_{best} values are not as good as that of spectroscopic redshifts, it is very useful for demographic studies, as our sample is nearly complete and the redshifts do not have the severe selection effects associated with

optical spectroscopy.

Subject headings: Gamma-Ray: Bursts – Cosmology: observations

1. Introduction

The redshifts have long been an important issue for long-duration Gamma-Ray Bursts (GRBs). Since the first X-ray, optical, and radio counterparts were discovered in 1997 (Costa et al. 1997; van Paradijs et al. 1997; Frail et al. 1997), GRBs are confirmed to be in galaxies at cosmological distances. However, until now, only a small fraction of the bursts have their redshifts measured. Even *Swift*, over its first four years of operation, has only roughly 30% of its bursts with spectroscopic/photometric redshifts. These redshifts may have complex selection biases as a function of redshift relating to the difficulty of getting redshifts for faint and distant bursts as well as the distribution of bands used for spectra and photometry. One illustration of the importance of the selection effects is that the average of redshift value for *Swift* GRBs have been dropped from $\langle z \rangle = 2.8$ (Jakobsson et al. 2006c) and to $\langle z \rangle = 2.1$ (Jakobsson 2008) while the average redshift value of earlier satellites is much lower yet (Bagoly et al. 2009). As the real redshift distribution of GRBs cannot be changed by that much for the past few years, the only reason for it would be changing selection effects in the spectroscopic observations.

These systematic biases will greatly affect various analyses. As long-duration GRBs come from the collapse of very massive fast-rotating stars with very short main-sequence lifetimes (Woosley & Bloom 2006), their rate density will provide a measurement of the massive star formation rate of our Universe. If we only deal with bursts with known spectroscopic redshifts, the derived star formation rate may be biased by the spectroscopic-redshift selection effects. The same problem comes with demographic studies of the GRB luminosity function. If only bursts with spectroscopic redshifts are used in constructing the luminosity functions, then the selection biases may distort the derived luminosity function. A third important problem is the recognition of the highest redshift bursts (say, with $z > 7$), against which the current spectroscopic methods may be heavily

biased. *Swift* is expected to have 5 – 10% of its bursts with $z > 7$ (Bromm & Loeb 2006), but the spectroscopic methods have only identified one such burst GRB090423, and that just a few month ago (Tanvir et al. 2009).

A solution to these problems is to use the luminosity relations that work on luminosity indicators measured directly from the prompt gamma-ray emission. These luminosity relations are equations that connect a measurable property of the burst itself (the luminosity indicators) to the bursts energy (E_γ or $E_{\gamma,iso}$) or the peak luminosity (L). The observed fluence or peak flux can then be used (with the inverse-square law) to derive a distance to the burst and (for some fiducial cosmology) the burst redshift. The advantage of this procedure is that it applies to all long class GRBs, not just to the minority selected to have a measured spectroscopic redshift. The disadvantage is that the uncertainties on the derived redshifts are much larger than those of the spectroscopic redshifts, and so the method can be used primarily for statistical or demographic purposes. The situation is similar to the case where photometric redshifts of distant galaxies in the Hubble Deep Field do not have the accuracy of the spectroscopic redshifts, yet nevertheless these photometric redshifts can be done for all the galaxies and are the cornerstone of all statistical studies of the field.

The six luminosity relations we use in this article are: τ_{lag} (spectral lag) - L relation (Norris, Marani, & Bonnell 2000), V (Variability) - L relation (Fenimore & Ramirez-Ruiz 2000), E_{peak} (peak energy of the spectrum) - L relation (Schaefer 2003b), $E_{peak} - E_\gamma$ relation (also called Ghirlanda relation, Ghirlanda, Ghisellini, & Lazzati (2004)), τ_{RT} (minimum rise time) - L relation (Schaefer 2002), and N_{peak} (number of peaks in the light curve) - L relation (Schaefer 2002). It was claimed by Butler et al. (2007) that the $E_{peak} - E_{\gamma,iso}$ relation (also called Amati relation, Amati et al. (2002)) differs somewhat between *Swift* and pre-*Swift* data, and hence the relation might be caused by the detection threshold effect of the instrument instead of the GRB itself. We tested this claim on the relations we

are using, as shown in Section 3.

In this article, we will demonstrate a method to use these luminosity relations to estimate the GRBs redshifts. Here, we will only consider bursts with known spectroscopic redshifts, but our derivation of z_{best} is based on the burst properties, and the effect of the known spectroscopic redshifts are negligible. This effect is tested later in the article. By applying our method to the bursts with accurate spectroscopic redshifts measured, we can compare our estimated redshifts with the measured spectroscopic redshifts. This will be the key test of our methods and the accuracy of our derived redshifts, as well as the applicability of our methods to bursts without spectroscopic redshift. With confidence in the reliability of the method, we can then apply it to all *Swift* bursts including those with no spectroscopic redshifts. Also, we will be able to apply this method to future bursts, and provide the community with a rapid notification about their redshifts. (Xiao & Schaefer 2009)

2. Improving the Luminosity Indicators

In this paper, we adopted five luminosity indicators with six luminosity relations (with two relations for indicator E_{peak} : $E_{peak} - L$ relation and $E_{peak} - E_{\gamma,iso}$ relation). The details of the calculations for each of these indicators are described in Schaefer (2007). In this paper, we constructed the calculation independently, and made some significant improvements in the calculation of τ_{lag} , τ_{RT} and N_{peak} . The five indicators are listed as below:

(1)The spectral lag, τ_{lag} , is the delay time between the soft and hard light curves of a burst. By convention, we use the soft and hard energy bands to be those of BATSE channels 1 and 3, or *Swift* channels 2 and 4, covering roughly 25-50 keV and 100-350 keV.

For τ_{lag} , by shifting the hard and soft light curves of a GRB, and calculating the cross correlation between them, we are able to get a cross-correlation versus offset plot. The offset corresponding with the peak value of the cross-correlation is the lag time we need. The calculation is simple and easy for bright bursts, while for those faint ones, since the plot has significant scatters, the offset with the peak correlation (i.e. τ_{lag}) is hard to evaluate under these noisy conditions. To find the offset when the cross-correlation achieves its peak value, we need to make a reasonable fit to the peak region of the cross correlation. As the shape and scatter of the plot varies from burst to burst, we cannot simply fit it with some specific function. If we fit it with a parabola, then any asymmetry in the cross correlation (as is often seen) will incorrectly shift the peak in the model by an amount depending on the range of offset included in the fit. And if we fit it with a high-order polynomial function, then the high-order terms will be unstable as they are trying to follow noise and regions far from the peak. What we did was to fit the cross correlation by polynomials with different orders (normally from 3 to 9), and choose the one which fits best in the very central region (around the peak) of the curve. Two examples are shown in Figure 1.

A bootstrap procedure is previously used to calculate the uncertainties on the τ_{lag} (Norris 2002). In our work, we are using a simple propagation method. The uncertainties on the cross-correlation amplitude points are calculated by simply evaluating the RMS scatters of these data points around the fitted curves. We are then able to generate the uncertainties for each of the fitting parameters, and the coefficient errors. Then the uncertainty for our τ_{lag} value, $\sigma_{\tau_{lag}}$, is generated by propagation of the uncertainties on the fitting parameters and the coefficients.

(2) Variability (V) measures whether a light curve is spiky or smooth, and can be obtained by calculating the normalized variance of the original light curve around the

smoothed light curve. The calculation of V is as shown in Schaefer (2007):

$$V = \langle [(C - C_{smooth})^2 - \sigma_C^2] / C_{smooth,max}^2 \rangle \quad (1)$$

where C is the count per time bin in the background subtracted light curve, with an uncertainty of σ_C . The time duration of the burst T_{up} is calculated as the summation of the time with the light curve brighter than 10% of its peak flux, and C_{smooth} is the count in the smoothed light curve, with a box-smoothing width to be 30% of T_{up} . $C_{smooth,max}$ is the peak value of C_{smooth} .

From equation (1), the $1 - \sigma$ uncertainty of V can be propagated from the observational uncertainty of C in each time bin. To get rid of the cross-correlation effect between C and C_{smooth} , for each C_i , we calculate it with

$$x_i = C_i - C_{i,smooth} = C_i - \frac{1}{N} \left(\sum_{j=i-N/2}^{i-1} C_j + \sum_{j=i+1}^{i+N/2} C_j \right) \quad (2)$$

where N is the box smooth bin (i.e. 30% of T_{up}).

If we neglect the uncertainty of σ_C , the $1 - \sigma$ uncertainty of V can be propagated from equation (1) and the uncertainties of each x_i and $C_{smooth,max}$.

The variability values (V) in Table 1 are about 10 times larger than those in Schaefer (2007). In this article, we are strictly following the definition and calculation of Equation (1). By checking the details of the calculation, we found that in Schaefer (2007), C_{max} was used in the denominator instead of $C_{smooth,max}$, which caused the difference. The values of variability are very sensitive to the slightly change on its calculation function, and this might be one of the reasons for the large scatter of the variability-luminosity relation.

(3) E_{peak} is the photon energy at which the νF_ν spectrum is the brightest. By fitting

the GRB spectrum with a smoothly broken power law (Band et al. 1993) as

$$\Phi(E) = \begin{cases} A E^\alpha e^{-(2+\alpha)E/E_{peak}} & \text{if } E \leq [(\alpha - \beta)/(2 + \alpha)]E_{peak} \\ B E^\beta & \text{otherwise} \end{cases} \quad (3)$$

the peak energy E_{peak} and corresponding parameters α (the asymptotic power law index for photon energies below the break) and β (the power law index for photon energies above the break) can be obtained. Here Φ is the usual differential photon spectrum (dN/dE) as a function of the photon energy (E). A GRB spectrum is also able to be fit with a power-law with exponential cutoff model:

$$dN/dE = A E^\alpha e^{-(2+\alpha)E/E_{peak}}, \quad (4)$$

with E_{peak} and power law index α being the fitting parameters. Here A and B are normalizing constants to indicate the brightness and constructed to ensure the continuity of the model spectrum.

In this article, we are using E_{peak} values of the bursts from various of sources. All the values we used and the sources are listed in Table 2.

(4)The minimum rise time in the light curve, τ_{RT} , was proposed for use in a luminosity relation by Schaefer (2002). The minimum rise time of a burst is taken to be the shortest time over which the light curve rises by half the peak flux of the pulse. In practice, especially for faint bursts with large Poisson noise, the rate difference between two close bins might be larger than half of the peak flux. As a result, we have to smooth the light curve before we calculate the rise time. The problem is then that if we smooth it too little, the apparent fastest rise time might be dominated by the Poisson noise, resulting in a too-small rise time, and if we smooth it too much, the smoothing effect will dominate, resulting in a rise time near the smoothing time bin.

As the light curves vary greatly among different bursts, there is no specific box smoothing width that can satisfy a majority of bursts. Instead, we vary the box smoothing

width from 0 bins (that is, no binning) up to a relatively large number, say 50 bins, and for each of these smoothing widths, we generate a smoothed lightcurve from which a minimum rise time can be calculated. Of course, some of these light curves are over-smoothed and some are under-smoothed. In a minimum rise time versus smoothing width plot, we will have a monotonically rising curve, as shown in Figure 2. Although the shape of the curve varies amongst bursts, for most of the bursts there will be a region where the curve appears flat, or with a slightly increasing slope, which we call a plateau. It is easy to explain the existence of the plateau: in this region, the smoothing is enough that Poisson noise is negligible in determining the minimum rise times, while the smoothing is not so much that it determines the minimum rise time. On a plot of minimum rise time versus smoothing width, we can identify three regions: a fast rising region where the Poisson noise dominates, a nearly flat plateau region where we are seeing the real minimum rise time, following by another rising region for large box smoothing widths where the smoothing is dominating. We can make use of this plateau region by extrapolating it back to the zero-smoothing case (where the box smoothing width is zero), as shown in Figure 2. The intercept on the y-axis corresponds with the minimum rise time where the smoothing is effectively zero. With the extrapolation, we are sidestepping the regime where the Poisson noise dominates. As a result, the value of the intercept is just the minimum rise time we need, not affected by either the Poisson noise effect or the smoothing effect.

For some of the extremely faint bursts, the Poisson noise dominant region and the smoothing effect dominant region will overlap with each other, and we are unable to find a plateau in the minimum rise time versus smooth width plot, for which the extrapolation cannot be made. Thus, our technique does not produce τ_{RT} values for the faintest bursts.

The uncertainty of the minimum rise time is calculated by simple propagation from the fitting parameters and the uncertainties on each individual point on the minimum rise

time versus smoothing width plot. The uncertainties on each of the individual points are dominated by the noise on each original data points in the light curve. The noise on the peak flux will affect our criteria, by some factor of $\sigma_C/\max(C)$, where C is the rate, and σ_C is the uncertainty of the rate. In addition to that, random noise on the start and stop data point for each possible rise time will affect our determination, i.e. the real rise time between two data points may be larger/smaller than half of the peak flux, however, with the random noise on the start and stop points, we take it as our rise time, which is equal to half of the peak flux. This effect is also reflected on our criteria also, by a factor of $\sim 2 * \sigma_C/\max(C)$. As a result, for determine the uncertainties on each of the individual rise time on RT-smoothing width plot, we can change our criteria from 0.5 by a factor of $2.25 * \sigma_C/\max(C)$, and record how much the resulted minimum rise time values changes. The uncertainties on the fitting parameters and the minimum rise time value can then be calculated from propagation.

(5) N_{peak} is defined as the number of peaks in the light curve. With C_{max} as the overall maximum of the background-subtracted light curve, we define a peak to be a local maximum that rises higher than $C_{max}/4$ and is also separated from all other peaks by a local minimum that is at least $C_{max}/4$ below the lower peak. In principle, N_{peak} is easy to count, either automatically or manually. In practice, we have the same problem of the Poisson noise and the smoothing factor effect, as what we had in the calculation of τ_{RT} . Faint bursts will have their unsmoothed light curves dominated by apparent peaks produced by Poisson noise, resulting in large numbers of false peaks. A random noise spike can satisfy our definition for a peak if we dont smooth the light curve, yet if we smooth it too much there will always be just one peak. Here we adopted the same procedure of calculation as that in the calculation of τ_{RT} . We vary the box smooth width from 0 bins to a relatively large number, and calculate the number of peaks for each of the smoothed light curves. As in the case for τ_{RT} , we see a fast falling curve (where Poisson noise is contributing spurious

peaks), with a plateau, where neither the Poisson noise effect nor the smoothing effect dominates. By extrapolating the plateau back to the y-axis, we get an N_{peak} value for an unsmoothed case of the light curve, with the effects of Poisson noise removed.

Each of the luminosity indicators discussed above has one or more corresponding luminosity relations. These relations are $\tau_{lag} - L$, $V - L$, $E_{peak} - L$, $E_{peak} - E_{\gamma}$ (so called Amati relation) and $E_{peak} - E_{\gamma,iso}$ (so called Ghirlanda relation), $\tau_{RT} - L$, and $N_{peak} - L$ relation, which are described and explained in details in Schaefer (2007). In our redshift calculation program, we are not including Amati relation for the following two reasons: First, the Amati relation has been challenged as it returns ambiguous redshifts (Li 2007), while the $E_{peak} - L$ relation (also the $\tau_{lag} - L$, $V - L$, $\tau_{RT} - L$, and $N_{peak} - L$ relations) passed the same test (Schaefer & Collazzi 2007). Second, the physics of the Amati relation is nearly the same as that of Ghirlandas $E_{peak} - E_{\gamma}$ relation, except that Ghirlandas $E_{peak} - E_{\gamma}$ relation has a correction for the jet opening angle, making it much tighter. There is another luminosity relation which relates E_{peak} , an effective duration (called T_{45}), and the luminosity by Firmani et al. (2006). However, with more GRBs and E_{peak} data added in, it is realized that this luminosity relation is not making any improvement on the $E_{peak} - L$ relation (Collazzi & Schaefer 2007).

3. Data for 107 Long GRBs and Six Luminosity Relations

We have 107 long GRBs with their spectroscopic/photometric redshifts measured, ranging from Feb. 28, 1997 (GRB970228) to July 21, 2008 (GRB080721), observed by BATSE, Konus, HETE, and *Swift*. The average redshift for pre-*Swift* bursts is about 1.50 and that of the *Swift* bursts is 2.15.

The light curves of *Swift* GRBs are generated from the original data published

on the legacy ftp site¹, and the *Swift* Software ver 2.9 (HEAsoft 6.5). To generate a background-subtracted light curve of a GRB, we downloaded an event file sw00xxxxxx000.bevshsp_uf.evt.gz and a mask file sw00xxxxxx000bcbdq.hk.gz, with xxxxxx be the six digit *Swift* trigger number. By running a task ‘batbinevt’, we can specify the time interval, energy bins, time bin method, output file name and format on generating the light curve. In our work, we adopted a time interval of 0.064 s with uniform time bins, and four continuous energy bands (15-25 keV, 25-50 keV, 50-100 keV and 100-350 keV). For the calculation of V , τ_{RT} and N_{peak} , we have been using the light curve over the whole energy range (15-350 keV), and for the calculation of τ_{lag} value, we use 25-50 keV and 100-350 keV. The light curves of pre-*Swift* bursts are obtained from our previous work (Schaefer 2007).

We calculated the τ_{lag} , V , τ_{RT} , and N_{peak} values for each of these bursts, as listed in Table 1. The first column lists the ID number of GRBs. The second column lists the satellite with the detection of the burst. Column three to six show all the calculated indicator values, with the name of the indicators shown on the header row. Indicators not measured due to low signal-to-noise ratio of the burst are represented as ‘...’.

The values of E_{peak} as well as the power law indexes α , β in Band’s smoothly broken power law model (Band et al. 1993) or E_{peak} and α values in a power law with exponential cutoff model are obtained from various sources, as shown in Table 2. The first column in Table 2 lists the ID number of the GRBs. The second column lists the satellite with the detection of the burst. Column three to six are the values of E_{peak} and the power law index α and β values, as well as the reference sources of these values. Our jet break time (t_{jet}) values from optical observations and their sources are also listed in Table 2, column seven and eight. Bursts without measured jet break time are filled by ‘...’ also. From the table we see that only 33 of the bursts have their optical t_{jet} reported. Various jet break time in

¹ftp://legacy.gsfc.nasa.gov/swift/data/obs

the X-ray afterglows have been reported, however, as there are usually multiple breaks for the X-ray afterglows, which are not well understood and distinguished for their causes, we are not including any of these reported t_{jet} values from X-ray detections. Values in square brackets for α and β are assumed values for those bursts without exact α and β values measured, which is taken to be the average value of known α and β (Schaefer et al. 1994; Krimm, et al. 2009; Kaneko et al. 2006; Band, et al. 1993). Some uncertainties of E_{peak} and t_{jet} are also quoted in square brackets. These uncertainties are assumed conservative assumed values, which are normally 10% of the measured E_{peak} or t_{jet} values. All of the peak flux (P) and fluence (S) values of pre-*Swift* bursts we use here are as same as what were used in Schaefer (2007), and those of *Swift* bursts are from the data table on the Swift webpage². All the quoted error bars in Table 1 and Table 2 are converted to $1 - \sigma$ level.

The luminosity relations are all expressed as power laws, and we can make a linear fit on the logarithms of the redshift-corrected luminosity indicators and the logarithms of the burst luminosities. In Figure 3, we display the data and the best fits for each of these luminosity relations, for the concordance cosmological model ($w = -1$, and $\Omega_M = 0.27$ in a flat universe). As there are significant uncertainties in both the horizontal and vertical axes, and some intrinsic scatters independent of both the luminosity and the redshift, we performed the ordinary least squares without any weighting (Isobe et al. 1990, Schaefer 2007). As both the indicator and luminosity are caused by some other parameter (like the jet Lorentz factor in particular), and so both indicator and luminosity are correlated. In this case, we assume that these two variables in the luminosity relations are not directly causative, and the bisector of the two ordinary least squares (Isobe et al. 1990) has been used. More details of the fitting process are referred to Schaefer (2007). As E_{peak} plays an important role in the calculation of P_{bolo} , the uncertainties on luminosity is then correlated

²http://swift.gsfc.nasa.gov/docs/swift/archive/grb_table/

with the uncertainties on E_{peak} . In our work, we ignored that effect, and simply assumed that P_{bolo} and E_{peak} have uncorrelated errors. The best fitting function for each of the relations are shown in Table 3.

The $V - L$ relation is rather scattered, as we can see from Figure 3 and Table 3. The scatter is larger than one could expect for any linear relations. As the calculation of V is not well defined, and $V - L$ relation is our most noisy luminosity relations. In this case, we decided not to include $V - L$ relation in our later calculation for the redshifts, although we listed all the calculated V values for the bursts in our Tables. As a result, the maximum number of luminosity indicators that we can use is 4, and the maximum number of luminosity relations is 5.

Butler et al. (2007) estimated the Amati’s relation ($E_{peak} - E_{\gamma,iso}$) with *Swift* and pre-*Swift* data. They report an inconsistency in the relations from the two data sets, which they then attributed to differences in threshold between *Swift* and earlier detectors. Their claimed difference has not been reproduced by other groups (including Cabrera et al. 2007; Schaefer 2007b; Krimm et al. 2009), while their claimed threshold effects have been found to not significantly affect the observed Amati relation (Schaefer 2007b; Nava et al. 2008; Ghirlanda et al. 2008; but see Shahmoradi & Nemiroff 2009). Indeed, their analysis is based on Bayesian priors which systematically push high- E_{peak} values below ~ 400 keV, as demonstrated by detailed comparisons with *Konus*, *Suzaku*, and *RHESSI* measures. Nevertheless, in this paper we can perform yet another test to see whether the claimed threshold differences between *Swift* and pre-*Swift* bursts cause any significant change in the luminosity relations. Butler et al. (2007) paper is including *Swift* BAT bursts between GRBs 041220 and 070509, 77 of which have spectroscopic redshift measured. While in our analysis on *Swift* GRBs, we are including all bursts with spectroscopic redshift between 050126 and 080721. With both samples being based on largely overlapping samples selected

in a nearly identical manner, we conclude that the flux limits of the two samples are essentially identical.

To this end, we have separately fitted the pre-*Swift* and *Swift* data. This test was only done for four luminosity relations ($\tau_{lag} - L$, $V - L$, $E_{peak} - L$, and $\tau_{RT} - L$), with the $E_{peak} - E_{\gamma}$ relation having too few bursts, and the $N_{peak} - L$ relation not being usable for the comparison as a limit. The best fit luminosity relations are given in Table 4. The data and best fit models are displayed in Figure 4. At first glance, we see that the difference between the two best fit lines are small compared to the scatter in the data, and a detailed analysis is described below.

We made a F-test for the fitting results for these four relations. First we made a bisector linear fit on the combined data with both pre-*Swift* and *Swift* bursts, and recorded the χ^2 value of the fit as χ^2_{JOINT} . Then we separate the data to two sample sets, pre-*Swift* and *Swift*, and made the same bisector linear fit separately on each set of the data. The sum of the two χ^2 values for the separately fitted lines are recorded as $\chi^2_{SEPARATE}$. Then the F value can be calculated as

$$F = \frac{\chi^2_{JOINT}/(N_{pre} + N_{sw} - 2)}{\chi^2_{SEPARATE}/(N_{pre} + N_{sw} - 4)} \quad (5)$$

where N_{pre} is the number of pre-*Swift* bursts, and N_{sw} is the number of *Swift* bursts. $N_{pre} + N_{sw} - 2$ is the degree of freedom of the fitting on the combined data, and $N_{pre} + N_{sw} - 4$ is the degrees of freedom of the fitting on separated data.

These F values for each of the luminosity relations are listed in Table 4. If the pre-*Swift* and *Swift* relations differ much from each other, the separate fitting have been significantly improved over the fitting on the mixed data, the F value would be much larger than unity. Otherwise, if there is no significant difference between pre-*Swift* and *Swift* relations, the F value would be around unity. From Table 4 we see that F is rather close to unity. All of the results shows that the separately fitted result is not significantly improved over the fitted

results on all data mixed together, which means that luminosity relations for pre-*Swift* luminosity relations and *Swift* luminosity relations do not significantly differ from each other. And by looking at the plots in Figure 4, we see that (1) the envelope of squares and diamonds are indistinguishable and (2) the pre-*Swift* and *Swift* best fit lines are close to each other compared to the scatter in the data. And hence, we have no significant evidence that these four luminosity relations differ for *Swift* bursts.

The $1 - \sigma$ range on the normalization difference between *Swift* and pre-*Swift* bursts for all these four luminosity relations are also listed in Table 4. We can make an analysis with the normalization difference on Amati’s relation claimed by Butler et al. (2007), which is corresponding with a 0.39 difference in log space. By making the comparison between the Butler’s factor (0.39) and our normalization difference, we can exclude Butlers factor at a 2.5 sigma level for $\tau_{lag} - L$ relation, a 3.7 sigma level for $\tau_{RT} - L$ relation, a 1.3 sigma level for $E_{peak} - L$ relation (which is not significant), and we cannot exclude the Butlers factor for $V - L$ relation.

4. Method for Calculating Redshift

Our aim in this paper is to test our method of redshift calculation. We applied it to the bursts with known spectroscopic redshifts (z_{spec}), and if it works well, we will be able to apply it to all the long GRBs in our future work. Although we are dealing with the bursts with known z_{spec} , these z_{spec} are only involved in the fitting of luminosity relations, and this effect is negligible in our calculation. Only after we have derived our redshift z_{best} from the luminosity relations will we compare them with the known z_{spec} to test our accuracy.

Below we will describe how our method applies on one Gamma-Ray Burst step by step:

(1) First, we measure each of the luminosity indicators of the burst. The definition and

method of calculations have been discussed in Sections 2 & 3. The results of the indicators for all bursts in the sample are listed in Table 1 & 2.

(2) We next derive the luminosity values for each relations from Table 3. A complexity is that the luminosity relations depend on the redshift of the burst (so as to correct the luminosity indicators back to the burst rest frame), so we have to perform this calculation for an array of trial redshifts (we take it to be from redshifts of 0 to 20 at intervals of 0.005), and then we will obtain a list of luminosities (or isotropic energies for Ghirlanda’s relation) values depending on the list of trial redshifts for each of the indicators. We notate each of these calculated luminosities (as a function of redshift z_{trial}) for the i th relation as $L_i(z_{trial})$ (or $E_{\gamma,i}$ for the Ghirlanda’s relation).

(3) With the values of the peak flux P , fluence S , E_{peak} and the power law indexes in the broken power law model α and β (or α from the power law with exponential cutoff model), the bolometric peak flux P_{bolo} and fluence S_{bolo} can be calculated. The range for ‘bolometric’ is set to be 1 keV to 10000 keV in the GRB rest frame, and the equations for the detailed calculation are referred to Schaefer (2007). As a result, for each burst, we calculated $P_{bolo}(z_{trial})$ and $S_{bolo}(z_{trial})$ for each trial redshift value from 0 to 20.

For those bursts with t_{jet} values, the jet opening angle θ_{jet} (in units of degrees) can be calculated as

$$\theta_{jet} = 0.161 * \left[\frac{t_{jet}}{1 + z_{trial}} \right]^{3/8} \left[\frac{n\eta_{\gamma}}{E_{\gamma,iso,52}} \right]^{1/8}, \quad (6)$$

where t_{jet} is the jet break time in the unit of days, n is the density of the circumburst medium in particles per cubic centimeter, η_{γ} is the radiative efficiency, and $E_{\gamma,iso,52}$ is the isotropic energy in units of 10^{52} erg (Rhoads 1997 & Sari et al. 1999). We simply adopt $\eta_{\gamma} = 0.2$ and $n = 3cm^{-3}$ in equation 6. The beaming factor F_{beam} , is then calculated as

$$F_{beam} = 1 - \cos \theta_{jet}. \quad (7)$$

From above we see that, since both θ_{jet} and $E_{\gamma,iso}$ are redshift sensitive, our calculated

F_{beam} value also varies between different z_{trial} values.

(4) From all the parameters above, for each of the indicators, a list of the luminosity distances can be calculated as

$$d_{L,i}(z_{trial}) = \sqrt{\frac{L_i(z_{trial})}{4\pi * P_{bolo}(z_{trial})}}. \quad (8)$$

For Ghirlanda's relation, the list of luminosity distances is calculated as

$$d_{L,i}(z_{trial}) = \sqrt{\frac{E_{\gamma,i}(z_{trial})[1 + z_{trial}]}{4\pi F_{beam} S_{bolo}(z_{trial})}}. \quad (9)$$

Then from each list of luminosity distance above, the distance modulus can be obtained:

$$\mu_i(z_{trial}) = 5 \log[d_{L,i}(z_{trial})] - 5, \quad (10)$$

with $d_{L,i}(z_{trial})$ expressed in units of parsecs. The uncertainties are propagated strictly following the calculation.

From all above, we are able to get up to four lists of measured distance moduli $\mu_i(z_{trial})$ with their $1 - \sigma$ uncertainties: $\mu_{\tau_{lag}} \pm \sigma_{\mu_{\tau_{lag}}}$, $\mu_{E_{peak}} \pm \sigma_{\mu_{E_{peak}}}$, $\mu_{E_{peak}-E_{\gamma}} \pm \sigma_{\mu_{E_{peak}-E_{\gamma}}}$, and $\mu_{\tau_{RT}} \pm \sigma_{\mu_{\tau_{RT}}}$. As we have asymmetric uncertainties for E_{peak} , we carry the uncertainties on both directions in the calculation, and generated both plus and minus uncertainties for $\mu_{E_{peak}}$ and $\mu_{E_{peak}-E_{\gamma}}$. $\mu_{N_{peak}}$ is also calculated, as a lower limit on the distance modulus. All of these distance moduli are a function of the assumed z_{trial} for $0 < z_{trial} < 20$.

(5) Given each trial redshift, we can calculate its distance modulus directly from the cosmological model, $\mu_{cos}(z_{trial})$. Here we adopt the concordance model, with equation of state for dark energy $p = w\rho c^2$, $w = -1$, $\Omega_M = 0.27$, $\Omega_{\Lambda} = 1 - \Omega_M = 0.73$, and $H_0 = 70(km/s)/Mpc$. In this case, the luminosity distance can be expressed as

$$d_L(z_{trial}) = cH_0^{-1}(1 + z_{trial}) \int_0^{z_{trial}} dz' [(1 + z')^3 \Omega_M + \Omega_{\Lambda}]^{-1/2}. \quad (11)$$

From the equation above and our list of trial redshifts, a list of luminosity distances $d_L(z_{trial})$ will be calculated, and also a list of distance modulus $\mu_{cos}(z_{trial})$ which equals $5 \log[d_L(z_{trial})] - 5$. The $\mu_{cos}(z_{trial})$ values are only depending on the trial redshift (running from 0 to 20) and the cosmological model we choose.

(6) For each of the trial redshifts from 0 to 20, we have distance moduli lists of $\mu_{\tau_{lag}}$, $\mu_{E_{peak}}$, $\mu_{E_{peak}-E_{\gamma}}$, $\mu_{\tau_{RT}}$ along with their $1 - \sigma$ uncertainties as well as μ_{cos} . We can then compare these $\mu_i(z_{trial})$ with $\mu_{cos}(z_{trial})$ in a χ^2 sense. Thus, $\chi_{\tau_{lag}}^2 = [(\mu_{\tau_{lag}} - \mu_{cos})/\sigma_{\mu_{\tau_{lag}}}]^2$ and so on for the other relations. We get a χ_i^2 versus z_{trial} plot, as shown in the left panel of Figure 5. Then sum over all the χ_i^2 , we get a χ_{total}^2 ($\chi_{total}^2 = \chi_{\tau_{lag}}^2 + \chi_{E_{peak}}^2 + \chi_{E_{peak}-E_{\gamma}}^2 + \chi_{\tau_{RT}}^2 + \chi_{N_{peak}}^2$) versus z_{trial} plot, as in the right panel of Figure 5. Our best redshift (z_{best}) corresponds with the minimum χ_{total}^2 , where the luminosity relations and the cosmological model agree with each other best. We are also able to find the uncertainties of our z_{best} . By searching through the $\chi_{total}^2 - z_{trial}$ plot, we can find the redshifts with which the $\chi_{total}^2 = \chi_{total,min}^2 + 1$, which corresponds with the edges of the $1 - \sigma$ range of our redshift. Similarly, the redshifts with $\chi_{total}^2 = \chi_{total,min}^2 + 4$ gives us the $2 - \sigma$ range and that with $\chi_{total}^2 = \chi_{total,min}^2 + 9$ gives the $3 - \sigma$ range of our redshift.

5. Results

The resulting values of z_{best} and $1 - \sigma$ range of z for each burst are shown in Table 5. We have also collected the spectroscopic redshifts for these bursts (see values and references in Table 5). The last column of Table 5 lists the effective luminosity relations we used for each burst in our calculation. The number of luminosity indicators used in the redshift calculation for each of the burst is listed in Table 5. A comparison can be made between our calculated redshifts and their spectroscopic (or photometric) redshifts. The comparison plot is shown in Figure 6, and below are some of the conclusions after we made the analysis:

(1) Of the total 115 bursts, 8 have only a lower z limit that can be calculated. For the remaining 107 bursts, we took the spectroscopic redshifts z_{spec} as the model value, and our calculated redshift z_{best} as a measured value, with the $1 - \sigma$ uncertainty of σ_{zPlus} and σ_{zMinus} . Then the χ^2 can be calculated as

$$\chi^2 = \sum_{j=1}^{N_{burst}} (z_{j,best} - z_{j,spec})^2 / \sigma_j^2, \quad (12)$$

with σ_j equals to $\sigma_{j,zPlus}$ or $\sigma_{j,zMinus}$, depending on whether our $z_{i,best}$ is smaller or larger than the $z_{i,spec}$. Each j represents an index number identifying the burst. The number of degrees of freedom in this comparison equals the number of bursts (N_{burst}), so the reduced χ^2 is χ^2 / N_{burst} . The reduced χ^2 value is 1.28, which is somewhat larger than unity. While after excluding one $3 - \sigma$ outliers GRB010222, whose contribution to χ^2 is as high as 44, our reduced χ^2 is equal to 0.86. This is certainly not a significant deviation from unity. So we conclude that the scatter in Figure 6 is consistent with our quoted error bars being correct.

(2) Of the 107 bursts with their z_{best} calculated, 73 has their z_{spec} falling into the $1 - \sigma$ range of our z . The ratio of the numbers is about 70%, which is slightly larger than the ideal case 68.5%. And for the 8 bursts with only lower z limit calculated, 6 of them have their z_{spec} larger than our $1 - \sigma$ lower limit of z . This is another way of testing our quoted error bars, and as in the previous item, we find no significant deviation from the expected results. As such, to a close degree, we see that our derived error bars are accurate.

(3) We can test to see whether our z_{best} is biased high or low. For this, we calculated the average value of $\log_{10}(z_{best}/z_{spec})$. If our result is unbiased, the average should be zero to within the error bars. We find the average is 0.01. This demonstrates that our z_{best} is not biased to within the 1% level.

(4) To test the accuracy of our z_{best} comparing with the z_{spec} , we calculated the RMS scatter of $\log_{10}(z_{best}/z_{spec})$. The result comes out to be 0.26, while the RMS scatter of

$\log_{10}(z_{spec})$ is 0.30. In Schaefer (2007) it was pointed out that the accuracy of the redshift estimation is 26% (corresponding to a $\log_{10}(z_{best}/z_{spec})$ RMS of 0.11), which is better than what we are claiming here. The reason for the larger RMS scatter is, although we are dealing with the GRBs with known z_{spec} , we are not making any use of the z_{spec} in our whole calculation, and our luminosity L , luminosity distance d_L , distance modulus μ_{ind} , as well as the bolometric flux and fluence P_{bolo} and S_{bolo} are all varying with our trial redshift. This brought us one extra degree of freedom in the calculation, which caused larger uncertainties in our result. When the known z_{spec} value is used (as for the Hubble diagram work in Schaefer 2007), the scatter becomes substantially small as compared to our work in this paper. Another reason for the large RMS is because it is mostly dominated by the very noise bursts (those bursts with low signal to noise ratio, inaccurate measurement of luminosity indicators, and large error bars for z_{best} results), which are not able to be used for the notification of the redshifts. If we make a selection on bursts with relatively accurate redshift estimation, say bursts with $\sigma_{z_{minus}/z_{best}} < 0.5$ and $\sigma_{z_{plus}/z_{best}} < 1$, we get the RMS of $\log(z_{best}/z_{spec})$ of 0.19, which is much smaller, and the RMS scatter of $\log_{10}(z_{spec})$ for this subsample is 0.28.

(5) We made the same calculation with pre-*Swift* luminosity relations on calculating *Swift* redshifts and *Swift* luminosity relations on calculating pre-*Swift* redshifts, for which we call it $z_{best,II}$. Our calculation on $z_{best,II}$ is totally independent on the spectroscopic redshifts, as for each burst, the luminosity relations used in the calculation are calibrated independent of the z_{spec} for any individual burst. The comparison between z_{best} and $z_{best,II}$ will also show the difference between *Swift* and pre-*Swift* luminosity relations. The comparison plot between z_{spec} and $z_{best,II}$ is shown on figure 7. From the comparison between figure 6 and figure 7 we see that, the scatter and distribution of z_{best} and $z_{best,II}$ do not differ significantly from each other. Actually, from our calculation, the average value of $\log_{10}(z_{best,II}/z_{spec})$ is -0.02, and the RMS scatter of $\log_{10}(z_{best,II}/z_{spec})$ is 0.27, both of

which are equal to those of our z_{best} value within error bars. This result demonstrate that those two sets of z_{best} values do not differ from each other, which means that these two sets of luminosity relations do not have significant difference. It also tells us that the effect of redshift involved in our calculation (in fitting luminosity relations) are negligible.

(6) We need to verify whether our result is effective in selecting high redshift bursts. If our predicted redshift is z , the possibility of a real redshift to be higher than z and lower than z are both 50%, which cannot be used as a test. However, by considering our uncertainties of z_{best} , if our predicted redshift is $2z$, we can make a test by counting how many of the GRBs are with real redshifts larger than z . As there are not many bursts with high redshifts, a test is done on a relatively lower redshift region, where most of the GRBs are involved. We picked up all our GRBs with predicted $z > 4$, the total number is 12, and 0 out of 12 have their spectroscopic redshift $z < 2$. This result tells us that our method is actually effective in demographic studies and in picking up high z bursts, if we take into the consideration of the error bars before we make the prediction.

From all the analysis above, we can conclude that our z_{best} is not biased on average, and our $1 - \sigma$ error bars are accurate. We can claim that our method works well on the bursts with known spectroscopic redshifts, and can be applied to all long GRBs (even without their z_{spec} measured).

6. Conclusions

In this paper, we developed a method to calculate the redshifts for long GRBs, using their light curves and spectra. We applied our method to bursts with known spectroscopic redshifts, detected by BATSE, HETE, Konus and *Swift*. By comparing our calculated redshifts with their spectroscopic redshifts, we are able to examine the accuracy of our

method.

We compared each of the luminosity relations for pre-*Swift* and *Swift* bursts by making a F-test. With the F values close to unity, we have significant evidence against any claim that the relations are caused by the detection threshold effects or any other artificial effects of the instruments.

We compared our results with the spectroscopic redshifts. We find that our z_{best} are not biased (with the average value of $\log_{10}(z_{best}/z_{spec})$ equal to 0.01), and our reported $1 - \sigma$ error bars are good (with $\chi_{red}^2 = 0.86$, and 70% of the z_{spec} fall into the $1 - \sigma$ region of z_{best}). Our accuracy on the redshifts are not as accurate as those from spectroscopy, yet nevertheless with a reasonable accuracy for demographical and statistical studies, with the RMS of $\log_{10}(z_{best}/z_{spec})$ is 0.26. The RMS value is about twice as what was found in Schaefer (2007). One of the reason is, in Schaefer (2007), the accuracy is calculated assuming a known z_{spec} , and in this paper, as we are treating the unknown-redshift case, so extra degrees of freedom has been brought in the calculation, which caused the accuracy to get worse by about a factor of 2. Another reason is that the large RMS is dominated by those faint and noisy burst, and for a subsample with $\sigma_{z_{minus}/z_{best}} < 0.5$ and $\sigma_{z_{plus}/z_{best}} < 1$, we get the RMS of $[\log(z_{best}/z_{spec})]$ of 0.19, which is much smaller. As our z_{best} are from the light curves, the spectra and the concordance cosmological model, it is independent of the spectroscopic redshift. As a result, our method can be applied to all long GRBs.

For *Swift* bursts, as we are measuring over a relatively narrow energy band (15 keV - 350 keV), the uncertainties in the calculation of peak energy E_{peak} is large, and it becomes one of the main restrictions on our accuracy. With the launch of Fermi, we are hoping to get bursts with more accurately measured E_{peak} values and light curves covering a broader energy band. We are expecting a substantial improvement in the accuracy of redshifts for Fermi bursts.

For the next step, we will apply our method to all *Swift* long GRBs, aiming to get a nearly-complete *Swift* GRBs redshift catalog. Such a catalog will inevitably be incomplete due to bursts with incomplete light curves and bursts too faint for their properties to be usefully measured. Our resulting redshifts will have an accuracy worse than those obtainable with optical spectroscopy, yet our accuracy will be good enough for various important statistical studies. As such, our catalog will be used for the demographic studies, without the detection threshold effect of the spectroscopic redshift measurements. We are also trying to deal with all the future bursts, and to provide a rapid notification of the redshift on the GCN circular to the community. We are hoping to find some possible high redshift (e.g. $z > 7$) and possible low redshift (e.g. $z < 0.3$) GRBs, which will be important in the observation of the high redshift universe and the GRB-SNe connection study.

This work is supported by NASA under grant NESSF 07Astro07F-0029.

REFERENCES

- Amati, L. et al. 2002, *A&A*, 390, 81.
- Amati, L., Frontera, F., Guidorzi, C., & Montanari, E. 2007, GCN 6017.
- Andersen, M. I. et al. 2000, *A&A*, 364, L54.
- Andersen, M. I., Masi, G., Jensen, B. L. & Hjorth, J. 2003, GCN 1993.
- Atteia, J.-L. et al. 2005, *ApJ*, 626, 292.
- Bagoly, Z., Balázs, L. G., Horváth, I., Kelemen, J., Mészáros, A., Veres, P., & Tusnády, G.,
2009, astro-ph/0901.0103.
- Band, D. et al. 1993, *ApJ*, 413, 281.
- Barbier, L. et al. 2006a, GCN 4518.
- Barbier, L. et al. 2006b, GCN 5974.
- Barthelmy, S. D. et al. 2008, GCN 7606.
- Berger, E. et al. 2003, *Nature*, 426, 154.
- Berger, E. et al. 2005a, GCN 3088.
- Berger, E. et al. 2005b, GCN 3368.
- Berger, E. & Becker, G. 2005, GCN 3520.
- Berger, E. et al. 2006a, GCN 4815.
- Berger, E. 2006, GCN 5962.
- Berger, E. & Gladders, M. 2006, GCN 5170.

Berger, E. & Shin, M.-S. 2006, GCN 5283.

Berger, E., Fox, D. B., & Cucchiara, A. 2007, GCN 6470.

Bloom, J. S., Berger, E., Kulkarni, S. R., Djorgovski, S. G., & Frail, D. A. 2003a, AJ, 125, 999.

Bloom, J. S., Frail, D. A., & Kulkarni, S. R. 2003b, ApJ, 594, 674.

Bloom, J. S., Foley, R. J., Kocevski, D., & Perley, D., 2006a, GCN 5217.

Bloom, J. S., Perley, D. A., & Chen, H.W. 2006, GCN 5826.

Blustin, A. J. et al. 2006, ApJ, 637, 901.

Bromm, V. & Loeb, A. 2006, ApJ, 642, 382.

Butler, N. R., Kocevski, D., Bloom, J. S., & Curtis, J. L. 2007, ApJ, 671, 656.

Cabrera, J. I., Firmani, C., Avila-Reese, V., Ghirlanda, G., Ghisellini, G., & Nava, L. 2007, MNRAS, 382, 342.

Calkins, M. 2000, IAUCirc. 7586, 1.

Castro-Tirado, A. J., Amado, P., Negueruela, I., Gorosabel, J., Jelnek, M., & Postigo, A. De Ugarte. 2006, GCN 5218.

Cenko, S. B. et al. 2005, GCN 3542.

Cenko, S. B. et al. 2006a, ApJ, 652, 490.

Cenko, S. B. et al. 2006b, GCN 5155.

Cenko, S. B. et al. 2007a, GCN 6556.

Cenko, S. B. et al. 2007b, GCN 6888.

Chen, H.-W. et al. 2005, GCN 3709.

Chornock, R. & Filippenko, A. V. 2002, GCN 1605.

Collazzi, A. C. & Schaefer, B. E., 2008, ApJ, 688, 456.

Costa, E. et al. 1997, Nature, 387, 783.

Cucchiara, A. et al. 2006a, GCN 4729.

Cucchiara, A. et al. 2006b, GCN 5052.

Cucchiara, A. et al. 2007, GCN 6083.

Cucchiara, A. et al. 2007b, GCN 7124.

Cucchiara, A. & Fox, D. B. 2008, GCN 7654.

Cummings, J. et al. 2006a, GCN 5621.

Cummings, J. et al. 2006b, GCN 5802.

Cummings, J. et al. 2007, GCN 6212.

Curran, P. A. et al. 2007, MNRAS, 381, L65.

Dai, X. & Stanek, Z. 2006, GCN 5147.

Djorgovski, S. G. et al. 1997, GCN 289.

Djorgovski, S. G., Kulkarni, S. R., Bloom, J. S., Goodrich, R., Frail, D. A., Piro, L., &
Palazzi, E. 1998, ApJ, 508, L17.

Djorgovski, S. G., Frail, D. A., Kulkarni, S. R., Bloom, J. S., Odewahn, S. C., & Diercks,
A. 2001a, ApJ, 562, 654.

Djorgovski, S. G. et al. 2001b, GCN 1108

Dodonov, S. N., Afanasiev, V. L., Sokolov, V. V., Moiseev, A. V., & Castro-Tirado A. J.
1999, GCN 475.

Dupre, A. K. et al. 2006, GCN 4969.

D’Elia, V. et al. 2006, GCN 5637.

D’Avanzo, P. et al. 2008, GCN 7997.

Fenimore, E. E. & Ramirez-Ruiz, E. 2000, astro-ph/0004176.

Ferrero, P. et al. 2009, A&A, 497, 729.

Filgas, R. et al. 2008, GCN 7747.

Firmani, C., Ghisellini, G., Avila-Reese, V., & Ghirlanda, G. 2006, MNRAS, 370, 185.

Foley, R. J., Chen H.-W., Bloom, J., & Prochaska, J. X. 2005, GCN 3483.

Frail, D. et al. 1997, Nature, 389, 261.

Fugazza, D. et al. 2004, GCN 2782.

Fugazza, D. et al. 2005, GCN 3948.

Fugazza, D. et al. 2006, GCN 5513.

Fynbo, J. P. U. et al. 2000, GCN 807.

Fynbo, J. P. U. et al. 2005a, GCN 3176.

Fynbo, J. P. U. et al. 2005b, GCN 3749.

Fynbo, J. P. U. et al. 2005c, GCN 3874.

Fynbo, J. P. U. et al. 2006a, GCN 4692.

Fynbo, J. P. U. et al. 2006b, GCN 5651.

Fynbo, J. P. U. et al. 2006c, GCN 5809.

Fynbo, J. P. U. et al. 2008a, GCN 7797.

Fynbo, J. P. U. et al. 2008b, GCN 7949.

Gal-Yam, A. et al. 2005, GCN 4156.

Ghirlanda, G., Ghisellini, G., & Lazzati, D. 2004, ApJ, 616, 331.

Ghirlanda, G., Nava, L., Ghisellini, G., Firmani, C. & Cabrera, J.I., 2007, MNRAS, 387,
319.

Golenetskii, S. et al. 2004, GCN 2754.

Golenetskii, S. et al. 2005a, GCN 4150.

Golenetskii, S. et al. 2005b, GCN 4238.

Golenetskii, S. et al. 2006a, GCN 4989.

Golenetskii, S. et al. 2006b, GCN 5460.

Golenetskii, S. et al. 2006c, GCN 5837.

Golenetskii, S. et al. 2007a, GCN 6879.

Golenetskii, S. et al. 2007b, GCN 7114.

Golenetskii, S. et al. 2008a, GCN 7482.

Golenetskii, S. et al. 2008b, GCN 7487.

Golenetskii, S. et al. 2008c, GCN 7589.

Golenetskii, S. et al. 2008d, GCN 7812.

Golenetskii, S. et al. 2008e, GCN 7854.

Golenetskii, S. et al. 2008f, GCN 7862.

Golenetskii, S. et al. 2008g, GCN 7995.

Graham, J. F. et al. 2007, GCN 6836.

Greiner, J. et al. 2003, GCN 2020.

Grupe D. et al. 2007, ApJ, 662, 443.

Guidorzi, C. et al. 2007, A&A, 463, 539.

Halpern, J. P. & Mirabal, N. et al. 2005, GCN 5982.

Hattori, T. et al. 2007, GCN 6444.

Hill, G., Prochaska, J. X., Fox, D., Schaefer, B., & Reed, M. 2005, GCN 4255.

Hjorth, J. et al. 2003, ApJ, 597, 699.

Holland, S. T. et al. 2003, AJ, 125, 2291.

Hurkett, C. P. et al. 2006, MNRAS, 368, 1101.

Isobe, T., Feigelson, E. D., Akritas, M. G., & Babu, G. J. 1990, ApJ, 364, 104.

Israel, G. et al. 1999, A&A, 348, L5.

Jakobsson, P. et al. 2004, A&A, 427, 785.

Jakobsson, P. et al. 2005a, GCN, 4029.

- Jakobsson, P. et al. 2005b, in AIP Conf. Proc. 836, Gamma-Ray Bursts in the Swift Era, Sixteenth Maryland Astrophysics Conference, ed. S.S. Holt, N. Gehrels, & J.A. Nousek (Washington, DC: AIP), 552.
- Jakobsson, P. et al. 2006a, GCN 5298.
- Jakobsson, P. et al. 2006b, GCN 5320.
- Jakobsson, P. et al. 2006c, A&A, 447, 897.
- Jakobsson, P. et al. 2007a, GCN 6283.
- Jakobsson, P. et al. 2007b, GCN 6398.
- Jakobsson, P. et al. 2007c, GCN 7117.
- Jakobsson, P. et al. 2008a, GCN 7286.
- Jakobsson, P. et al. 2008b, GCN 7757.
- Jakobsson, P. et al. 2008c, GCN 7832.
- Jakobsson, P., Malesani, D., Fynbo, J. P. U., Hjorth, J. & Milvang-Jensen, B., 2008d, in AIP Conf. Proc. 1133, Gamma-Ray Bursts, 6th GRB Huntsville Symposium, ed. C. Meegan, N. Gehrels & C. Kouveliotou (Huntsville, AL: AIP), 455.
- Jaunsen, A.O. et al. 2007a, GCN 6010.
- Jaunsen, A.O. et al. 2007b, GCN 6216.
- Jimenez, R., Band, D., & Piran, T. 2001, ApJ, 561, 171.
- Kaneko, Y., Preece, R. D., Briggs, M. S., Paciesas, W. S., Meegan, C. A., & Band, D. L., 2006, ApJSupp, 166, 298.

Kann, D. A. et al. 2007, GCN 6935.

Kelson, D. D., Illingworth, G. D., Franx, M., Magee, D., & van Dokkum, P. G., 1999,
IAUCirc. 7096, 3

Kelson, D., & Berger, E. 2005, GCN 3101.

Klose, S. et al. 2004, AJ, 128, 1942.

Kobayashi, S., Ryde, F., & MacFadyen, A. 2002, ApJ, 577, 302.

Krimm, H. et al. 2006a, in Gamma-Ray Bursts in the Swift Era, eds S. S. Holt, N. Gehrels,
and J. A. Nousek (AIP Conf. Proc. 836), pp. 145-148.

Krimm, H. A. et al. 2007, ApJ, 665, 554.

Krimm, H. et al. 2009, ApJ, in press, arXiv:0908.1335.

Kulkarni, S. R. et al. 1998, Nature, 393, 35.

Kulkarni, S. R. et al. 1999, Nature, 398, 389.

Le Floch, E. et al. 2002, ApJ, 581, L81.

Ledoux, C. et al. 2006, GCN 5237.

Ledoux, C. et al. 2007, GCN 7023.

Levan, A. et al. 2006, ApJ, 647, 471.

Li, L. 2007, MNRAS, 374, L20.

Li, W., Jha, S., Filippenko, A. V., Bloom, J. S., Pooley, D., Foley, R. J., & Perley, D. A.
2005, GCN 4095.

- Liang, E.-W., Racusin, J. L., Zhang, B., Zhang, B.-B., & Burrows, D. N. 2008, *ApJ*, 675, 528.
- Malesani, D., et al. 2007, GCN 6343.
- Malesani, D., et al. 2008, GCN 7544.
- Markwardt, C. et al. 2006, GCN 5520.
- Markwardt, C. et al. 2007a, GCN 6081.
- Markwardt, C. et al. 2007b, GCN 6274.
- Martini, P., Garnavich, P., & Stanek, K. Z. 2003, GCN 1980.
- Melandri, A., Grazian, A., Guidorzi, C., Monfardini, A., Mundell, C.G., & Gomboc, A. 2006, GCN 4539.
- Mészáros, P., Ramirez-Ruiz, E., Rees, M. J., & Zhang, B. 2002, *ApJ*, 578, 812.
- Metzger, M. R., Djorgovski, S. G., Kulkarni, S. R., Steidel, C. C., Adelberger, K. L., Frail, D. A., Costa, E., & Frontera, F. 1997, *Nature*, 387, 878.
- Moretti, A. et al. 2006, GCN 5194.
- Nava, L., Ghirlanda, G., Ghisellini, G. & Firmani, C., 2008, *MNRAS*, 391, 639.
- Norris, J. P., Marani, G. F., & Bonnell, J. T. 2000, *ApJ*, 534, 248.
- Norris, J. P., 2002, *ApJ*, 579, 386.
- Ohno, M. & Tueller, J. et al. 2008, GCN 7630.
- Osip, D. et al. 2006, GCN 5715.
- Page et al. 2007, *ApJ*, 663, 1125.

Palmer, D. et al. 2006, GCN 4697.

Parsons, A. et al. 2006a, GCN 5370.

Parsons, A. et al. 2006b, GCN 5561.

Perley, D. A., et al. 2007, GCN 6850.

Peterson, B. et al. 2006, GCN 5223.

Piranomonte, S. et al. 2006, GCN 4520.

Piro, L. et al. 2002, ApJ, 577, 680.

Price, P. A. et al. 2002a, ApJ, 573, 85.

Price, P. A., Bloom, J. S., Goodrich, R. W., Barth, A. J., Cohen, M. H., & Fox, D. W.
2002b, GCN 1475.

Price, P. A. et al. 2003a, ApJ, 589, 838.

Price, P. A. et al. 2003b, GCN 1889.

Price, P. A. et al. 2006, GCN 5104.

Prochaska, J. X., Bloom, J. S., Wright, J. T., Butler, R. P., Chen, H. W., Vogt, S. S., &
Marcy, G. W. 2005b, GCN 3833.

Prochaska, J. X., Thoene, C. C., Malesani, D., Fynbo, J. P. U., & Vreeswijk, P. M., 2007a,
GCN 6698.

Prochaska, J. X. et al. 2007b, GCN 6864.

Prochaska, J. X. et al. 2008a, GCN 7388.

Prochaska, J. X. et al. 2008b, GCN 7849.

- Quimby, R., Fox, D., Hoefflich, P., Roman, B., & Wheeler, J. C. 2005, GCN 4221.
- Racusin, J. et al. 2005, GCN 4169.
- Rau, A., Salvato, M., & Greiner, J. 2005, A&A, 444, 425.
- Rhoads, J. E. 1997, ApJ, 487, L1.
- Rykoff et al. 2006, ApJ, 638, L5.
- Rol, E. et al. 2006, GCN 5555.
- Sakamoto, T. et al. 2005, ApJ, 629, 311.
- Sakamoto, T. et al. 2006, ApJ, 636, L73.
- Sakamoto, T. et al. 2008, ApJS, 175, 179.
- Sari, R., Piran, T., & Halpern, J. P. 1999, ApJ, 519, L17.
- Schady, P. et al. 2006, ApJ, 643, 276
- Schaefer, B. E. et al. 1994, ApJSupp, 92, 285.
- Schaefer, B. E. 2002, Gamma-Ray Bursts: The Brightest Explosions in the Universe (Harvard).
- Schaefer, B. E. & Collazzi, A. C. 2007, ApJ, 656, L53.
- Schaefer, B. E. 2007a, ApJ, 660, 16.
- Schaefer, B. E. 2007b, BAAS, 39, 743.
- Shahmoradi, A. & Nemiroff, R. J. 2009, arXiv:0904.1464.
- Soderberg, A. M. et al. 2005, GCN 4186.

Stamatikos, M. et al. 2006, GCN 5810.

Stamatikos, M. et al. 2007, GCN 6326.

Stanek, K. Z. et al. 2005, ApJ, 626, L5.

Tanvir, N. et al. 2009, Nature, in press, arXiv: astro-ph/0906.1577.

Tagliaferri, G. et al. 2005, A&A, 443, L1.

Thoene, C. C. et al. 2006a, GCN 5373.

Thoene, C. C. et al. 2006b, GCN 5812.

Thoene, C. C., Jaunsen, A. O., Fynbo, J. P. U., Jakobsson, P., & Vreeswijk, P. M., 2007a, GCN 6379.

Thoene, C. C., Jakobsson, P., Fynbo, J. P. U., Malesani, D., Hjorth, J., & Vreeswijk, P. M., 2007b, GCN 6499.

Thoene, C. C., Perley, D. A., Cooke, J., Bloom, J. S., Chen, H.-W., & Barton, E., 2007, GCN 6741.

Thoene, C. C., De Cia, A., Malesani, D., & Vreeswijk, P. M. 2008a, GCN 7587.

Thoene, C. C. et al. 2008b, GCN 7602.

Thoene, C. C. et al. 2008c, astro-ph/0806.1182.

Ulanov, M. V., Golenetskii, S. V., Frederiks, D. D., Mazets, R. L., Aptekar E. P., Kokomov, A. A., & Palshin, V. D. 2005, Nuovo Cimento C, 28, 351.

van Paradijs, J. et al. 1997, Nature, 386, 686.

Vreeswijk, P. M. et al. 1999a, GCN 324.

Vreeswijk, P. M. et al. 1999b, GCN 496.

Vreeswijk, P. M. et al. 2002, GCN 1785

Vreeswijk, P. M. et al. 2003, GCN 1953.

Vreeswijk, P. M. et al. 2008a, GCN 7444.

Vreeswijk, P. M. et al. 2008b, GCN 7601.

Weidinger, M. et al. 2003, GCN 2215.

Wiersema, K. et al. 2004, GCN 2800.

Wiersema, K. et al. 2008, GCN 7517.

Woosley, S. E. & Bloom, J. S. 2006, ARA&A, 44, 507.

Xiao, L. & Schaefer, B. E., 2008, in AIP Conf. Proc. 1133, Gamma-Ray Bursts, 6th GRB
Huntsville Symposium, ed. C. Meegan, N. Gehrels & C. Kouveliotou (Huntsville,
AL: AIP), 486.

Yost S. A. et al. 2007, ApJ, 2007, 657, 925.

Zhang, B., Zhang, B.-B., Liang, E.-W., Gehrels, N., Burrows, D. N., & Mészáros, P. 2007,
ApJ, 655, L25.

Table 1. Luminosity Indicators.

<i>GRB</i>	Satellite	$\tau_{lag}(\text{sec})$	V	$\tau_{RT}(\text{sec})$	N_{peak}
970228	Konus	...	0.016 ± 0.010	...	2
970508	BATSE	0.49 ± 0.02	0.018 ± 0.004	0.65 ± 0.07	1
970828	Konus	...	0.052 ± 0.005	0.36 ± 0.14	4
971214	BATSE	0.03 ± 0.05	0.048 ± 0.002	...	2
980703	BATSE	0.69 ± 0.02	0.024 ± 0.001	3.00 ± 0.19	1
990123	BATSE	0.07 ± 0.01	0.059 ± 0.003	...	3
990506	BATSE	0.04 ± 0.01	0.337 ± 0.001	0.13 ± 0.01	12
990510	BATSE	0.03 ± 0.01	0.118 ± 0.001	0.13 ± 0.01	8
990705	Konus	...	0.097 ± 0.004	0.62 ± 0.37	4
991208	Konus	...	0.023 ± 0.003	0.27 ± 0.01	4
991216	BATSE	0.03 ± 0.01	0.062 ± 0.003	0.09 ± 0.01	5
000131	Konus	...	0.056 ± 0.005	0.84 ± 0.39	2
000210	Konus	...	0.018 ± 0.002	0.45 ± 0.03	1
000911	Konus	...	0.122 ± 0.013	0.07 ± 0.22	5
000926	Konus	...	0.326 ± 0.034	...	4
010222	Konus	...	0.143 ± 0.004	0.45 ± 0.01	6
010921	HETE	1.00 ± 0.04	0.008 ± 0.006	4.31 ± 0.71	1
020124	HETE	0.07 ± 0.06	0.266 ± 0.040	0.59 ± 0.17	3
020405	Konus	...	0.104 ± 0.007	0.48 ± 0.09	2
020813	HETE	0.15 ± 0.01	0.164 ± 0.004	0.59 ± 0.05	5
021004	HETE	0.71 ± 0.19	0.035 ± 0.067	1.23 ± 0.96	2
021211	HETE	0.31 ± 0.01	0.006 ± 0.003	0.57 ± 0.01	1
030115	HETE	0.44 ± 0.06	0.020 ± 0.020	0.70 ± 0.40	1
030226	HETE	0.31 ± 0.22	0.033 ± 0.029	1.76 ± 1.15	3
030323	HETE	...	0.021 ± 0.338	...	2
030328	HETE	0.08 ± 0.08	0.024 ± 0.003	1.69 ± 0.81	2
030329	HETE	0.15 ± 0.01	0.065 ± 0.002	0.66 ± 0.01	2
030429	HETE	0.03 ± 0.17	0.220 ± 0.135	...	2
030528	HETE	12.56 ± 0.14	0.017 ± 0.010	2.13 ± 0.42	1
040924	HETE	0.90 ± 0.01	0.060 ± 0.003	0.33 ± 0.17	1
041006	HETE	...	0.050 ± 0.002	1.28 ± 0.01	3
050408	HETE	0.31 ± 0.02	0.082 ± 0.005	0.49 ± 0.02	1

Table 1—Continued

<i>GRB</i>	Satellite	$\tau_{lag}(\text{sec})$	V	$\tau_{RT}(\text{sec})$	N_{peak}
051022	Konus	...	0.088 ± 0.008	0.19 ± 0.04	1
050126	Swift	2.74 ± 0.02	-0.010 ± 0.065	1.58 ± 1.91	1
050223	Swift	...	0.111 ± 0.094	...	1
050315	Swift	...	0.032 ± 0.016	1.97 ± 1.62	2
050401	Swift	0.06 ± 0.02	0.187 ± 0.019	0.25 ± 0.16	3
050406	Swift	...	0.020 ± 0.274	...	2
050416A	Swift	...	0.021 ± 0.030	0.54 ± 0.06	1
050505	Swift	0.71 ± 0.13	0.076 ± 0.031	0.60 ± 0.21	3
050525A	Swift	0.12 ± 0.01	0.093 ± 0.003	0.32 ± 0.01	2
050603	Swift	-0.01 ± 0.01	0.125 ± 0.014	0.19 ± 0.01	1
050730	Swift	...	0.027 ± 0.066	...	2
050802	Swift	...	0.070 ± 0.036	2.03 ± 1.02	4
050814	Swift	...	-0.009 ± 0.180	...	2
050820A	Swift	...	0.061 ± 0.033	1.01 ± 0.75	3
050824	Swift	...	0.289 ± 0.640	...	1
050826	Swift	...	0.063 ± 0.105	1.11 ± 2.28	1
050908	Swift	...	-0.017 ± 0.046	1.10 ± 1.47	1
050922C	Swift	0.06 ± 0.01	0.015 ± 0.003	0.13 ± 0.01	2
051016B	Swift	...	0.008 ± 0.030	...	2
051109A	Swift	...	-0.006 ± 0.025	0.70 ± 1.25	1
051111	Swift	1.70 ± 0.07	0.009 ± 0.004	1.80 ± 0.24	1
060108	Swift	...	0.006 ± 0.040	...	2
060115	Swift	...	0.019 ± 0.029	1.11 ± 1.71	2
060206	Swift	0.01 ± 0.03	0.007 ± 0.004	1.16 ± 0.18	1
060210	Swift	0.15 ± 0.17	0.183 ± 0.033	0.73 ± 0.50	4
060223A	Swift	...	0.036 ± 0.021	0.41 ± 0.23	4
060418	Swift	0.22 ± 0.03	0.104 ± 0.008	0.67 ± 0.08	2
060502A	Swift	4.90 ± 0.11	0.004 ± 0.010	2.94 ± 1.19	1
060510B	Swift	...	0.110 ± 0.060	...	4
060512	Swift	...	0.043 ± 0.173	...	1
060522	Swift	...	0.034 ± 0.185	...	1
060526	Swift	0.17 ± 0.09	0.085 ± 0.030	0.38 ± 0.11	2

Table 1—Continued

<i>GRB</i>	Satellite	$\tau_{lag}(\text{sec})$	V	$\tau_{RT}(\text{sec})$	N_{peak}
060604	Swift	...	0.080 ± 0.338	...	2
060605	Swift	...	-0.013 ± 0.068	1.22 ± 0.72	3
060607A	Swift	1.98 ± 0.11	0.025 ± 0.008	1.23 ± 0.68	1
060707	Swift	...	0.050 ± 0.054	...	2
060714	Swift	...	0.125 ± 0.022	...	≥ 3
060729	Swift	...	0.092 ± 0.041	...	2
060814	Swift	0.29 ± 0.03	0.040 ± 0.003	1.65 ± 0.24	2
060904B	Swift	0.36 ± 0.09	0.003 ± 0.008	1.00 ± 0.16	1
060908	Swift	0.26 ± 0.06	0.061 ± 0.008	0.52 ± 0.09	3
060926	Swift	1.03 ± 0.11	0.148 ± 0.050	...	2
060927	Swift	0.12 ± 0.04	0.094 ± 0.010	0.46 ± 0.12	2
061007	Swift	0.11 ± 0.01	0.066 ± 0.003	0.38 ± 0.02	4
061110A	Swift	...	-0.038 ± 0.050	...	1
061110B	Swift	0.24 ± 0.36	0.155 ± 0.064	0.79 ± 0.64	9
061121	Swift	0.03 ± 0.01	0.050 ± 0.003	0.98 ± 0.19	2
061222B	Swift	...	0.024 ± 0.043	...	2
070110	Swift	...	-0.010 ± 0.031	...	1
070208	Swift	...	0.083 ± 0.211	...	2
070318	Swift	...	0.037 ± 0.008	0.72 ± 0.24	1
070411	Swift	...	0.041 ± 0.029	...	2
070506	Swift	2.52 ± 0.04	0.010 ± 0.030	0.12 ± 0.06	1
070508	Swift	0.04 ± 0.01	0.106 ± 0.003	0.20 ± 0.01	4
070521	Swift	0.04 ± 0.01	0.116 ± 0.004	0.58 ± 0.06	5
070529	Swift	...	0.170 ± 0.091	...	1
070611	Swift	...	0.053 ± 0.080	...	1
070612A	Swift	...	0.032 ± 0.023	2.49 ± 1.48	2
070714B	Swift	0.03 ± 0.01	0.164 ± 0.021	0.45 ± 0.04	1
070802	Swift	...	-0.156 ± 0.150	...	1
070810A	Swift	1.09 ± 0.23	-0.006 ± 0.015	0.73 ± 0.22	1
071003	Swift	0.38 ± 0.05	0.072 ± 0.007	0.88 ± 0.07	4
071010A	Swift	...	-0.076 ± 0.153	...	1
071010B	Swift	0.84 ± 0.04	0.010 ± 0.003	1.21 ± 0.03	1

Table 1—Continued

<i>GRB</i>	Satellite	$\tau_{lag}(\text{sec})$	V	$\tau_{RT}(\text{sec})$	N_{peak}
071031	Swift	...	-0.038 ± 0.108	...	2
071117	Swift	0.60 ± 0.01	0.009 ± 0.003	0.20 ± 0.02	1
071122	Swift	...	0.391 ± 0.392	...	1
080210	Swift	0.53 ± 0.17	0.019 ± 0.013	0.57 ± 0.44	3
080310	Swift	...	0.038 ± 0.021	0.41 ± 0.55	3
080319B	Swift	0.02 ± 0.01	0.031 ± 0.003	0.14 ± 0.01	10
080319C	Swift	...	0.042 ± 0.007	0.21 ± 0.12	4
080330	Swift	...	0.109 ± 0.060	...	3
080411	Swift	0.21 ± 0.01	0.167 ± 0.003	0.65 ± 0.01	2
080413A	Swift	0.13 ± 0.03	0.078 ± 0.004	0.23 ± 0.03	3
080413B	Swift	0.23 ± 0.01	0.004 ± 0.003	0.50 ± 0.03	1
080430	Swift	0.68 ± 0.08	0.009 ± 0.004	0.76 ± 0.12	1
080516	Swift	0.15 ± 0.01	0.168 ± 0.055	...	2
080520	Swift	...	0.037 ± 0.098	...	1
080603B	Swift	0.08 ± 0.01	0.283 ± 0.010	0.22 ± 0.03	6
080605	Swift	0.11 ± 0.01	0.057 ± 0.003	0.22 ± 0.01	4
080607	Swift	0.04 ± 0.01	0.035 ± 0.003	0.18 ± 0.06	6
080707	Swift	...	0.093 ± 0.032	...	2
080721	Swift	0.13 ± 0.05	0.048 ± 0.009	0.09 ± 0.04	4

Table 2. Luminosity Indicators.

<i>GRB</i>	Satellite	E_{peak} (keV) ^a	α^a	β^a	Ref. ^b	t_{jet} (day)	Ref. ^b
970228	Konus	115^{+38}_{-38}	-1.54 ± 0.08	-2.5 ± 0.4
970508	BATSE	389^{+40}_{-40}	$-1.19 \pm [0.1]$	$-1.83 \pm [0.4]$	2	25.00 ± 5.00	40
970828	Konus	298^{+30}_{-30}	$-0.704 \pm [0.1]$	$-2.07 \pm [0.4]$	2	2.20 ± 0.40	40
971214	BATSE	190^{+20}_{-20}	$-0.78 \pm [0.1]$	$-2.57 \pm [0.4]$	2
980703	BATSE	254^{+25}_{-25}	$-1.31 \pm [0.1]$	$-2.4 \pm [0.4]$	2	3.40 ± 0.50	40
990123	BATSE	604^{+60}_{-60}	$-0.9 \pm [0.1]$	$-2.48 \pm [0.4]$	2	2.04 ± 0.46	41
990506	BATSE	283^{+30}_{-30}	$-1.37 \pm [0.1]$	$-2.15 \pm [0.4]$	2
990510	BATSE	126^{+10}_{-10}	$-1.28 \pm [0.1]$	$-2.67 \pm [0.4]$	2	1.60 ± 0.20	42
990705	Konus	189^{+15}_{-15}	-1.05 ± 0.21	-2.2 ± 0.1	1	1.00 ± 0.20	40
991208	Konus	190^{+20}_{-20}	$[-1.1] \pm [0.4]$	$[-2.2] \pm [0.4]$	3
991216	BATSE	318^{+30}_{-30}	$-1.23 \pm [0.1]$	$-2.18 \pm [0.4]$	2	1.20 ± 0.40	40
000131	Konus	163^{+13}_{-13}	-1.2 ± 0.1	-2.4 ± 0.1	4
000210	Konus	408^{+14}_{-14}	$[-1.1] \pm [0.4]$	$[-2.2] \pm [0.4]$	5
000911	Konus	986^{+100}_{-100}	$-0.84 \pm [0.1]$	$[-2.2] \pm [0.4]$	6
000926	Konus	100^{+7}_{-7}	$[-1.1] \pm [0.4]$	$-2.43 \pm [0.4]$	5
010222	Konus	309^{+12}_{-12}	-1.35 ± 0.19	-1.64 ± 0.02	5	0.93 ± 0.10	40
010921	HETE	89^{+22}_{-14}	-1.6 ± 0.1	$[-2.2] \pm [0.4]$	7
020124	HETE	87^{+18}_{-12}	$-0.8^{+0.2}_{-0.1}$	$[-2.2] \pm [0.4]$	7	3.00 ± 0.40	43
020405	Konus	364^{+90}_{-90}	$[-1.1] \pm [0.4]$	-1.87 ± 0.2	8	1.67 ± 0.52	44
020813	HETE	140^{+14}_{-13}	-0.94 ± 0.03	$-1.57^{+0.03}_{-0.04}$	7	0.43 ± 0.06	40
021004	HETE	80^{+53}_{-23}	-1 ± 0.2	$[-2.2] \pm [0.4]$	7	4.74 ± 0.50	45
021211	HETE	46^{+8}_{-6}	-0.9 ± 0.1	$-2.2^{+0.1}_{-0.3}$	7
030115	HETE	83^{+53}_{-22}	-1.3 ± 0.1	$[-2.2] \pm [0.4]$	7
030226	HETE	97^{+27}_{-17}	-0.9 ± 0.2	$[-2.2] \pm [0.4]$	7	1.04 ± 0.12	46
030323	HETE	44^{+90}_{-26}	-0.8 ± 0.8	$[-2.2] \pm [0.4]$	9
030328	HETE	130^{+14}_{-13}	-1.14 ± 0.03	$-2.1^{+0.2}_{-0.4}$	7	0.80 ± 0.10	47
030329	HETE	68^{+2}_{-2}	-1.26 ± 0.02	-2.28 ± 0.06	7	0.50 ± 0.10	43
030429	HETE	35^{+12}_{-8}	$-1.1^{+0.3}_{-0.2}$	$[-2.2] \pm [0.4]$	7	1.77 ± 1.00	48
030528	HETE	32^{+5}_{-5}	$-1.3^{+0.2}_{-0.1}$	$-2.7^{+0.3}_{-1.0}$	7
040924	HETE	67^{+6}_{-6}	$-1.17 \pm [0.1]$	$[-2.2] \pm [0.4]$	10, 11
041006	HETE	63^{+13}_{-13}	$-1.37 \pm [0.1]$	$[-2.2] \pm [0.4]$	11	0.16 ± 0.04	49
050126	Swift	47^{+23}_{-8}	$[-1.1] \pm [0.4]$	$[-2.2] \pm [0.4]$	12

Table 2—Continued

<i>GRB</i>	Satellite	E_{peak} (keV) ^a	α^a	β^a	Ref. ^b	t_{jet} (day)	Ref. ^b
050223	Swift	62_{-10}^{+10}	$-1.46 \pm [0.1]$	$[-2.2] \pm [0.4]$	13
050315	Swift	39_{-7}^{+7}	$[-1.1] \pm [0.4]$	$[-2.2] \pm [0.4]$	14
050401	Swift	118_{-18}^{+18}	-0.9 ± 0.3	-2.55 ± 0.3	15
050406	Swift	25_{-13}^{+35}	$[-1.1] \pm [0.4]$	-2.56 ± 0.35	16
050408	HETE	$[100]_{-50}^{+[100]}$	$[-1.1] \pm [0.4]$	$[-2.2] \pm [0.4]$
050416A	Swift	15_{-3}^{+2}	$[-1.1] \pm [0.4]$	-3.4 ± 0.4	17
050505	Swift	70_{-24}^{+140}	-0.31 ± 1	$[-2.2] \pm [0.4]$	12
050525A	Swift	81_{-1}^{+1}	-1.01 ± 0.06	-3.26 ± 0.2	15	0.40 ± 0.10	50, 51
050603	Swift	344_{-52}^{+52}	-1.03 ± 0.06	-2.03 ± 0.1	15
050730	Swift	124_{-26}^{+26}	$[-1.1] \pm [0.4]$	$[-2.2] \pm [0.4]$	14
050802	Swift	121_{-28}^{+28}	$[-1.1] \pm [0.4]$	$[-2.2] \pm [0.4]$	14
050814	Swift	60_{-6}^{+24}	0 ± 0.6	$[-2.2] \pm [0.4]$	18
050820A	Swift	246_{-40}^{+76}	-1.25 ± 0.1	$[-2.2] \pm [0.4]$	15	$18^s \pm 2.00$	52
050824	Swift	15_{-5}^{+5}	$[-1.1] \pm [0.4]$	$[-2.2] \pm [0.4]$	14
050826	Swift	105_{-47}^{+47}	$[-1.1] \pm [0.4]$	$[-2.2] \pm [0.4]$	14
050908	Swift	41_{-5}^{+9}	$[-1.1] \pm [0.4]$	$[-2.2] \pm [0.4]$	12
050922C	Swift	198_{-22}^{+38}	-0.95 ± 0.07	$[-2.2] \pm [0.4]$	15	0.11 ± 0.03	53
051016B	Swift	24_{-7}^{+7}	$[-1.1] \pm [0.4]$	$[-2.2] \pm [0.4]$	14
051022	Konus	510_{-20}^{+22}	-1.18 ± 0.02	$[-2.2] \pm [0.4]$	19	2.90 ± 0.20	54
051109A	Swift	161_{-35}^{+130}	$-1.25_{-0.36}^{+0.27}$	$[-2.2] \pm [0.4]$	20	0.60 ± 0.10	55
051111	Swift	220_{-48}^{+1703}	-1 ± 0.18	$[-2.2] \pm [0.4]$	18	0.0080 ± 0.0003	56
060108	Swift	65_{-10}^{+600}	$[-1.1] \pm 0.4$	$[-2.2] \pm [0.4]$	13
060115	Swift	62_{-6}^{+19}	-1 ± 0.3	$[-2.2] \pm [0.4]$	21
060206	Swift	78_{-8}^{+23}	-1.2 ± 0.18	$[-2.2] \pm [0.4]$	22	0.57 ± 0.06	57, 58
060210	Swift	149_{-35}^{+400}	-1.18 ± 0.03	$[-2.2] \pm [0.4]$	13
060223A	Swift	71_{-10}^{+100}	-1.18 ± 0.31	$[-2.2] \pm [0.4]$	13
060418	Swift	$230_{-20}^{+[20]}$	$-1.5 \pm [0.1]$	$[-2.2] \pm [0.4]$	23
060502A	Swift	156_{-33}^{+400}	-1.18 ± 0.15	$[-2.2] \pm [0.4]$	13
060510B	Swift	$95_{-30}^{+[60]}$	-1.47 ± 0.18	$[-2.2] \pm [0.4]$	13
060512	Swift	22_{-6}^{+6}	$[-1.1] \pm [0.4]$	$[-2.2] \pm [0.4]$	14
060522	Swift	80_{-12}^{+382}	-0.7 ± 0.48	$[-2.2] \pm [0.4]$	18
060526	Swift	$25_{-5}^{+[5]}$	$[-1.1] \pm [0.4]$	$[-2.2] \pm [0.4]$	13	2.41 ± 0.06	59

Table 2—Continued

<i>GRB</i>	Satellite	E_{peak} (keV) ^a	α^a	β^a	Ref. ^b	t_{jet} (day)	Ref. ^b
060604	Swift	40^{+5}_{-5}	$-1.34 \pm [0.3]$	$[-2.2] \pm [0.4]$	13
060605	Swift	90^{+91}_{-12}	-0.3 ± 0.42	$[-2.2] \pm [0.4]$	18	0.24 ± 0.02	60
060607A	Swift	120^{+190}_{-17}	-1.06 ± 0.18	$[-2.2] \pm [0.4]$	13
060707	Swift	63^{+13}_{-6}	-0.6 ± 0.42	$[-2.2] \pm [0.4]$	22
060714	Swift	103^{+21}_{-16}	$[-1.1] \pm [0.4]$	$[-2.2] \pm [0.4]$	24	$0.12 \pm [0.01]$	24
060729	Swift	61^{+9}_{-9}	$[-1.1] \pm [0.4]$	$[-2.2] \pm [0.4]$	25	0.50 ± 0.06	61
060814	Swift	257^{+74}_{-35}	-1.43 ± 0.09	$[-2.2] \pm [0.4]$	26
060904B	Swift	80^{+770}_{-12}	-1 ± 0.42	$[-2.2] \pm [0.4]$	18
060908	Swift	151^{+112}_{-25}	-1 ± 0.18	$[-2.2] \pm [0.4]$	22
060926	Swift	20^{+11}_{-11}	$[-1.1] \pm [0.4]$	$[-2.2] \pm [0.4]$	14
060927	Swift	72^{+15}_{-7}	-0.9 ± 0.24	$[-2.2] \pm [0.4]$	22
061007	Swift	399^{+12}_{-11}	-0.7 ± 0.02	-2.61 ± 0.09	14
061110A	Swift	90^{+13}_{-13}	$[-1.1] \pm [0.4]$	$[-2.2] \pm [0.4]$	14
061110B	Swift	517^{+53}_{-53}	$[-1.1] \pm [0.4]$	$[-2.2] \pm [0.4]$	14
061121	Swift	606^{+55}_{-44}	$-1.32^{+0.02}_{-0.03}$	$[-2.2] \pm [0.4]$	27	$1.16 \pm [0.16]$	62
061222B	Swift	49^{+8}_{-8}	$[-1.1] \pm [0.4]$	$[-2.2] \pm [0.4]$	14
070110	Swift	110^{+30}_{-30}	$[-1.1] \pm [0.4]$	$[-2.2] \pm [0.4]$	28
070208	Swift	51^{+10}_{-10}	$[-1.1] \pm [0.4]$	$[-2.2] \pm [0.4]$	14
070318	Swift	154^{+19}_{-19}	$[-1.1] \pm [0.4]$	$[-2.2] \pm [0.4]$	14
070411	Swift	83^{+11}_{-11}	$[-1.1] \pm [0.4]$	$[-2.2] \pm [0.4]$	14
070506	Swift	31^{+2}_{-3}	-5.00 ± 1.82	2.01 ± 0.22	18
070508	Swift	233^{+7}_{-7}	-0.96 ± 0.13	$[-2.2] \pm [0.4]$	14
070521	Swift	222^{+16}_{-12}	-0.93 ± 0.07	$[-2.2] \pm [0.4]$	14
070529	Swift	180^{+52}_{-52}	$[-1.1] \pm [0.4]$	$[-2.2] \pm [0.4]$	14
070611	Swift	92^{+30}_{-30}	$[-1.1] \pm [0.4]$	$[-2.2] \pm [0.4]$	14
070612A	Swift	87^{+17}_{-17}	$[-1.1] \pm [0.4]$	$[-2.2] \pm [0.4]$	14
070714B	Swift	1120^{+473}_{-230}	-0.86 ± 0.06	$[-2.2] \pm [0.4]$	14
070802	Swift	70^{+25}_{-25}	$[-1.1] \pm [0.4]$	$[-2.2] \pm [0.4]$	14
070810A	Swift	44^{+9}_{-9}	$[-1.1] \pm [0.4]$	$[-2.2] \pm [0.4]$	14
071003	Swift	799^{+75}_{-61}	-0.97 ± 0.04	$[-2.2] \pm [0.4]$	14
071010A	Swift	27^{+10}_{-10}	$[-1.1] \pm [0.4]$	$[-2.2] \pm [0.4]$	14
071010B	Swift	52^{+6}_{-8}	$-1.25^{+0.45}_{-0.30}$	$-2.65^{+0.18}_{-0.30}$	29	3.44 ± 0.39	63

Table 2—Continued

<i>GRB</i>	Satellite	E_{peak} (keV) ^a	α^a	β^a	Ref. ^b	t_{jet} (day)	Ref. ^b
071031	Swift	24_{-7}^{+7}	$[-1.1] \pm [0.4]$	$[-2.2] \pm [0.4]$	14
071117	Swift	278_{-48}^{+143}	-1.53 ± 0.09	$[-2.2] \pm [0.4]$	30
071122	Swift	73_{-30}^{+30}	$[-1.1] \pm [0.4]$	$[-2.2] \pm [0.4]$	14
080210	Swift	73_{-15}^{+15}	$[-1.1] \pm [0.4]$	$[-2.2] \pm [0.4]$	14
080310	Swift	28_{-6}^{+6}	$[-1.1] \pm [0.4]$	$[-2.2] \pm [0.4]$	14
080319B	Swift	651_{-8}^{+8}	-0.82 ± 0.01	$-3.87_{-0.66}^{+0.27}$	31
080319C	Swift	307_{-56}^{+85}	-1.01 ± 0.08	$-1.87_{-0.38}^{+0.09}$	32
080330	Swift	20_{-9}^{+9}	$[-1.1] \pm [0.4]$	$[-2.2] \pm [0.4]$	14
080411	Swift	259_{-16}^{+21}	$-1.51_{-0.03}^{+0.02}$	$[-2.2] \pm [0.4]$	33
080413A	Swift	170_{-24}^{+48}	-1.20 ± 0.06	$[-2.2] \pm [0.4]$	34
080413B	Swift	73_{-10}^{+10}	-1.26 ± 0.16	$[-2.2] \pm [0.4]$	35
080430	Swift	80_{-15}^{+15}	$[-1.1] \pm [0.4]$	$[-2.2] \pm [0.4]$	14
080516	Swift	66_{-24}^{+24}	$[-1.1] \pm [0.4]$	$[-2.2] \pm [0.4]$	14
080520	Swift	12_{-5}^{+5}	$[-1.1] \pm [0.4]$	$[-2.2] \pm [0.4]$	14
080603B	Swift	85_{-18}^{+55}	$-0.94_{-0.45}^{+0.73}$	$-1.96 \pm [0.4]$	36
080605	Swift	246_{-11}^{+14}	-1.02 ± 0.06	$[-2.2] \pm [0.4]$	37
080607	Swift	394_{-33}^{+35}	-1.06 ± 0.05	$[-2.2] \pm [0.4]$	38
080707	Swift	73_{-20}^{+20}	$[-1.1] \pm [0.4]$	$[-2.2] \pm [0.4]$	14
080721	Swift	485_{-36}^{+41}	$-0.93_{-0.05}^{+0.06}$	$-2.43_{-0.25}^{+0.15}$	39

^aThe values reported in square brackets are conservative estimations for uncertainties not reported in the original paper.

^bReferences. —(1) Amati et al. 2002; (2) Jimenez, Band, & Piran 2001; (3) Golenetskii 2005, private communication; (4) Andersen et al. 2000; (5) Ulanov et al. 2005; (6) Price et al. 2002a; (7) Sakamoto et al. 2005; (8) Price et al. 2003a; (9) Atteia et al. 2005; (10) Golenetskii et al. 2004; (11) HETE Bursts 2006, available at <http://space.mit.edu/HETE/Bursts/>; (12) Krimm 2005, private communication; (13) Krimm 2006, private communication; (14) calculated from the relation in Zhang et al. 2007; (15) Krimm et al. 2006a; (16) Schady et al. 2006; (17) Sakamoto et al. 2006; (18) Butler et al. 2007; (19) Golenetskii et al. 2005a; (20) Golenetskii et al. 2005b; (21) Barbier et al. 2006a; (22) Sakamoto et al. 2008; (23) Golenetskii et al. 2006a; (24) Krimm et al. 2007; (25) Rykoff et al. 2006; (26) Golenetskii et al. 2006b; (27) Golenetskii et al. 2006c; (28) Amati et al. 2007; (29) Golenetskii et al. 2007a; (30) Golenetskii et al. 2007b; (31) Golenetskii

et al. 2008a; (32) Golenetskii et al. 2008b; (33) Golenetskii et al. 2008c; (34) Ohno et al. 2008; (35) Barthelmy et al. 2008; (36) Golenetskii et al. 2008d; (37) Golenetskii et al. 2008e; (38) Golenetskii et al. 2008f; (39) Golenetskii et al. 2008g; (40) Bloom et al. 2003b; (41) Kulkarni et al. 1999; (42) Israel et al. 1999; (43) Berger et al. 2003; (44) Price et al. 2003a; (45) Holland et al. 2003; (46) Klose et al. 2004; (47) Andersen et al. 2003; (48) Jakobsson et al. 2004; (49) Stanek et al. 2005; (50) Liang et al. 2008; (51) Mirebel et al. 2007; (52) Cenko et al. 2006a; (53) Li et al. 2005; (54) Racusin et al. 2005; (55) Yost et al. 2007; (56) Guidozi et al. 2007; (57) Curran et al. 2007; (58) Stenik et al. 2005; (59) Thoene et al. 2008c; (60) Ferrero et al. 2009; (61) Grupe et al. 2007; (62) Page et al. 2007; (63) Kann et al. 2007;

Table 3. Luminosity Relations

Indicator	Relation	σ_a^a	σ_b^a	σ_{sys}^a
τ_{lag}	$\log L = 52.21 - 0.98 \log[\tau_{lag}(1+z)^{-1}/0.1s]$	0.04	0.03	0.48
V	$\log L = 51.06 + 1.35 \log[V(1+z)/0.02]$	0.09	0.09	0.87
E_{peak}	$\log L = 52.10 + 1.88 \log[E_{peak}(1+z)/300keV]$	0.03	0.01	0.57
E_{peak}	$\log E_\gamma = 50.57 + 1.63 \log[E_{peak}(1+z)/300keV]$	0.09	0.03	0.16
τ_{RT}	$\log L = 52.84 - 1.70 \log[\tau_{RT}(1+z)^{-1}/0.1s]$	0.04	0.05	0.53
N_{peak}	$\log L \geq 50.32 + 2 \log[N_{peak}]$ for $N_{peak} \geq 2$

^aThe σ_a , σ_b are the $1 - \sigma$ uncertainties of the fitting parameters, while a is the intercept on the y-axis, and b is the slope of the fitting line. σ_{sys} is the systematic uncertainty added in quadrature to the measurement errors, with which the χ_{red}^2 of the points about the best fit line is unity.

Table 4. Comparison of Luminosity Relations

Luminosity Relation	pre-Swift burst	Swift burst	F	$\sigma_{norm,diff}^a$
τ_{lag} -L	$\log L = 52.14 - 0.95 \log[\tau_{lag}(1+z)^{-1}/0.1s]$	$\log L = 52.26 - 1.00 \log[\tau_{lag}(1+z)^{-1}/0.1s]$	0.98	0.11
Variability-L	$\log L = 51.38 + 1.24 \log[V(1+z)/0.02]$	$\log L = 50.92 + 1.34 \log[V(1+z)/0.02]$	1.04	0.09
E_{peak} -L	$\log L = 51.42 + 1.71 \log[E_{peak}(1+z)/300keV]$	$\log L = 51.13 + 1.88 \log[E_{peak}(1+z)/300keV]$	1.02	0.08
τ_{RT} -L	$\log L = 52.87 - 1.44 \log[\tau_{RT}(1+z)^{-1}/0.1s]$	$\log L = 52.81 - 1.85 \log[\tau_{RT}(1+z)^{-1}/0.1s]$	1.00	0.18

^aThe $\sigma_{norm,diff}$ is the $1 - \sigma$ range of the difference of normalization values between *Swift* and pre-*Swift* luminosity relations. It is calculated by $\sqrt{\sigma_{norm,preSwift}^2 + \sigma_{norm,Swift}^2}$.

Table 5. Our Redshifts and Spectroscopic Redshifts.

<i>GRB</i>	Experiment	z_{spec}	Ref. ^a	z_{best}	z_{min}	z_{max}	N_{rel}
970228	Konus	0.84	1	0.38	0.18	0.86	2
970508	BATSE	0.84	2	1.51	1.11	2.09	4
970828	Konus	0.96	3	1.10	0.73	1.83	4
971214	BATSE	3.42	4	5.21	2.00	20	3
980703	BATSE	0.97	5	0.84	0.66	1.11	4
990123	BATSE	1.61	6	0.91	0.67	1.27	4
990506	BATSE	1.31	7	1.16	0.77	1.84	4
990510	BATSE	1.62	8	2.47	1.69	3.66	5
990705	Konus	0.84	9	0.63	0.45	0.94	4
991208	Konus	0.71	10	0.46	0.29	0.78	3
991216	BATSE	1.02	11	0.60	0.47	0.79	5
000131	Konus	4.50	12	1.75	0.90	4.41	3
000210	Konus	0.85	13	0.59	0.35	1.04	2
000911	Konus	1.06	14	2.88	1.06	18.31	3
000926	Konus	2.07	15	0.60	0.31	1.41	2
010222	Konus	1.48	16	0.45	0.35	0.61	4
010921	HETE	0.45	17	0.40	0.28	0.59	3
020124	HETE	3.20	18	5.27	3.24	8.12	5
020405	Konus	0.70	19	0.90	0.64	1.32	4
020813	HETE	1.25	20	0.98	0.72	1.36	5
021004	HETE	2.32	21	2.41	1.53	4.06	5
021211	HETE	1.01	22	0.71	0.49	1.07	3
030115	HETE	2.50	23	2.24	1.34	4.12	3
030226	HETE	1.98	24	2.39	1.59	3.58	5
030323	HETE	3.37	25	1.52	0.55	20	2
030328	HETE	1.52	26	1.28	0.80	2.34	5
030329	HETE	0.17	27	0.24	0.19	0.29	5
030429	HETE	2.66	28	4.62	2.41	8.25	4
030528	HETE	0.78	29	0.77	0.53	1.14	3
040924	HETE	0.86	30	0.61	0.42	0.91	3
041006	HETE	0.71	31	0.64	0.48	0.89	4
050126	Swift	1.29	32	1.64	1.00	2.91	3

Table 5—Continued

<i>GRB</i>	Experiment	z_{spec}	Ref. ^a	z_{best}	z_{min}	z_{max}	N_{rel}
050223	Swift	0.59	33	2.80	0.94	20	1
050315	Swift	1.95	34	0.82	0.45	1.78	3
050401	Swift	2.90	35	2.02	1.23	3.63	4
050406	Swift	2.44	36	1.68	0.71	20	2
050408	HETE	1.24	37	1.43	0.90	2.40	3
050416A	Swift	0.65	38	0.73	0.43	1.33	2
050505	Swift	4.27	39	2.73	1.68	4.67	4
050525A	Swift	0.61	40	0.92	0.71	1.21	5
050603	Swift	2.82	41	1.24	0.69	2.69	2
050730	Swift	3.97	42	> 2.53			2
050802	Swift	1.71	43	1.09	0.61	2.41	3
050814	Swift	5.30	44	2.70	0.89	20.00	2
050820A	Swift	2.61	45	2.97	1.96	4.80	4
050824	Swift	0.83	46	0.61	0.30	1.50	1
050826	Swift	0.30	47	> 2.42			2
050908	Swift	3.35	48	2.02	0.84	9.23	2
050922C	Swift	2.20	49	1.51	1.20	1.90	5
051016B	Swift	0.94	50	0.65	0.32	1.52	2
051022	Konus	0.80	51	0.95	0.66	1.51	3
051109A	Swift	2.35	52	1.33	0.74	2.34	3
051111	Swift	1.55	53	1.09	0.79	1.48	4
060108	Swift	2.03	54	2.96	0.74	20	2
060115	Swift	3.53	55	2.63	0.99	20	3
060206	Swift	4.05	56	1.73	0.93	4.02	4
060210	Swift	3.91	57	2.54	1.95	3.97	4
060223A	Swift	4.41	58	> 2.06			3
060418	Swift	1.49	59	1.41	0.92	2.25	4
060502A	Swift	1.51	60	0.86	0.55	1.37	3
060510B	Swift	4.90	61	> 1.72			2
060512	Swift	0.44	62	0.64	0.31	1.69	1
060522	Swift	5.11	63	7.24	1.08	20	1
060526	Swift	3.21	64	3.50	2.07	6.57	5

Table 5—Continued

<i>GRB</i>	Experiment	z_{spec}	Ref. ^a	z_{best}	z_{min}	z_{max}	N_{rel}
060604	Swift	2.68	65	2.72	0.97	20	2
060605	Swift	3.80	66	6.79	1.96	20	4
060607A	Swift	3.08	67	1.47	0.92	2.48	3
060707	Swift	3.43	68	2.15	0.78	20	2
060714	Swift	2.71	69	3.77	1.09	20	3
060729	Swift	0.54	70	1.66	0.81	3.48	3
060814	Swift	0.84	71	0.93	0.63	1.43	4
060904B	Swift	0.70	72	1.89	0.81	5.46	3
060908	Swift	2.43	73	2.13	1.30	3.84	4
060926	Swift	3.21	74	1.44	0.83	2.71	3
060927	Swift	5.60	75	3.24	1.81	6.44	4
061007	Swift	1.26	76	0.94	0.65	1.42	4
061110A	Swift	0.76	77	> 1.82			1
061110B	Swift	3.44	78	8.28	3.35	20	4
061121	Swift	1.31	79	0.79	0.58	1.11	5
061222B	Swift	3.36	80	1.10	0.50	3.68	2
070110	Swift	2.35	81	> 1.995			1
070208	Swift	1.17	82	1.76	0.70	10.15	2
070318	Swift	0.84	83	3.42	1.43	18.32	2
070411	Swift	2.95	84	2.73	1.53	4.72	2
070506	Swift	2.31	85	2.73	1.80	4.38	3
070508	Swift	0.82	86	1.25	0.81	2.02	4
070521	Swift	0.55	87	2.08	1.27	3.73	4
070529	Swift	2.50	88	> 1.67			1
070611	Swift	2.04	89	5.55	1.24	20	1
070612A	Swift	0.62	90	1.82	0.85	5.61	3
070714B	Swift	0.92	91	3.12	1.74	6.97	3
070802	Swift	2.45	92	9.37	1.51	20	1
070810A	Swift	2.17	93	1.53	0.97	2.56	3
071003	Swift	1.10	94	0.83	0.56	1.25	4
071010A	Swift	0.98	95	0.86	0.38	2.88	1
071010B	Swift	0.95	96	0.76	0.53	1.12	4

Table 5—Continued

<i>GRB</i>	Experiment	z_{spec}	Ref. ^a	z_{best}	z_{min}	z_{max}	N_{rel}
071031	Swift	2.69	97	1.10	0.52	3.40	2
071117	Swift	1.33	98	1.13	0.76	1.74	3
071122	Swift	1.14	99	> 1.05			1
080210	Swift	2.64	100	2.35	1.37	4.42	4
080310	Swift	2.43	101	1.19	0.60	3.22	3
080319B	Swift	0.94	102	1.45	0.95	2.34	4
080319C	Swift	1.95	103	3.62	1.31	20	3
080330	Swift	1.51	104	0.79	0.37	1.94	2
080411	Swift	1.03	105	0.51	0.36	0.74	4
080413A	Swift	2.43	106	2.42	1.47	4.36	4
080413B	Swift	1.10	107	0.73	0.50	1.11	3
080430	Swift	0.77	108	1.56	1.00	2.60	3
080516	Swift	3.20	109	3.62	1.86	7.96	3
080520	Swift	1.55	110	0.52	0.25	1.21	1
080603B	Swift	2.69	111	4.55	2.40	9.88	4
080605	Swift	1.64	112	1.06	0.71	1.65	4
080607	Swift	3.04	113	1.32	0.82	2.29	4
080707	Swift	1.23	114	2.35	0.77	20	2
080721	Swift	2.60	115	1.13	0.72	1.86	4

^aReferences. — (1) Djorgovski et al. 1997; (2) Metzger et al. 1997; (3) Djorgovski et al. 2001a; (4) Kulkarni et al. 1998; (5) Djorgovski et al. 1998a; (6) Kelson et al. 1999; (7) Bloom et al. 2003a; (8) Vreeswijk et al. 1999a; (9) Le Floch et al. 2002; (10) Dodonov et al. 1999; (11) Vreeswijk et al. 1999b; (12) Andersen et al. 2000; (13) Piro et al. 2002; (14) Price et al. 2002b; (15) Fynbo et al. 2000; (16) Calkins 2000; (17) Djorgovski et al. 2001b; (18) Hjorth et al. 2003; (19) Masetti et al. 2002; (20) Price et al. 2002a; (21) Chornock & Filippenko 2002; (22) Vreeswijk et al. 2002; (23) Levan et al. 2006; (24) Price et al. 2003b; (25) Vreeswijk et al. 2003; (26) Martini et al. 2003; (27) Greiner et al. 2003; (28) Weidinger et al. 2003; (29) Rau, Salvato, & Greiner 2005; (30) Wiersema et al. 2004; (31) Fugazza et al. 2004; (32) Berger et al. 2005a; (33) Berger & Min-Su Shin 2006; (34) Kelson & Berger

2005; (35) Fynbo et al. 2005a; (36) Schady et al. 2006; (37) Berger et al. 2005c; (38) Cenko et al. 2005; (39) Berger et al. 2005b; (40) Foley et al. 2005; (41) Berger & Becker 2005; (42) Chen et al. 2005; (43) Fynbo et al. 2005b; (44) Jakobsson et al. 2005b; (45) Prochaska et al. 2005b; (46) Fynbo, et al. 2005c; (47) Halpern & Mirabal et al. 2005; (48) Fugazza et al. 2005; (49) Jakobsson et al. 2005a; (50) Soderberg et al. 2005; (51) Gal-Yam et al. 2005; (52) Quimby et al. 2005; (53) Hill et al. 2005; (54) Melandri et al. 2006; (55) Piranomonte et al. 2006; (56) Fynbo et al. 2006a; (57) Cucchiara et al. 2006a; (58) Berger et al. 2006a; (59) Dupre et al. 2006; (60) Cucchiara et al. 2006b; (61) Price et al. 2006; (62) Bloom et al. 2006a; (63) Cenko et al. 2006b; (64) Berger & Gladders 2006; (65) Castro-Tirado et al. 2006; (66) Peterson et al. 2006; (67) Ledoux et al. 2006; (68) Jakobsson et al. 2006a; (69) Jakobsson et al. 2006b; (70) Thoene et al. 2006a; (72) Fugazza et al. 2006; (73) Rol et al. 2006; (74) D’Elia, et al. 2006; (75) Fynbo et al. 2006b; (76) Osip et al. 2006; (77) Thoene et al. 2006b; (78) Fynbo et al. 2006c; (79) Bloom et al. 2006; (80) Berger 2006; (81) Jaunsen et al. 2007a; (82) Cucchiara et al. 2007; (83) Jaunsen et al. 2007b; (84) Jakobsson et al. 2007a; (85) Thoene et al. 2007a; (86) Jakobsson et al. 2007b; (87) Hattori et al. 2007; (88) Berger et al. 2007; (89) Thoene et al. 2007b; (90) Cenko et al. 2007a; (91) Graham et al. 2007; (92) Prochaska et al. 2007a; (93) Thoene et al. 2007c; (94) Perley et al. 2007; (95) Prochaska, J. X. et al. 2007b; (96) Cenko et al. 2007b; (97) Ledoux et al. 2007; (98) Jakobsson et al. 2007c; (99) Cucchiara et al. 2007b; (100) Jakobsson et al. 2008a; (101) Prochaska, et al. 2008a; (102) Vreeswijk et al. 2008a; (103) Wiersema et al. 2008; (104) Malesani et al. 2008; (105) Thoene et al. 2008a; (106) Thoene et al. 2008b; (107) Vreeswijk et al. 2008b; (108) Cucchiara & Fox 2008; (109) Filgas et al. 2008; (110) Jakobsson et al. 2008b; (111) Fynbo et al. 2008a; (112) Jakobsson et al. 2008c; (113) Prochaska, et al. 2008b; (114) Fynbo et al. 2008b; (115) D’Avanzo et al. 2008;

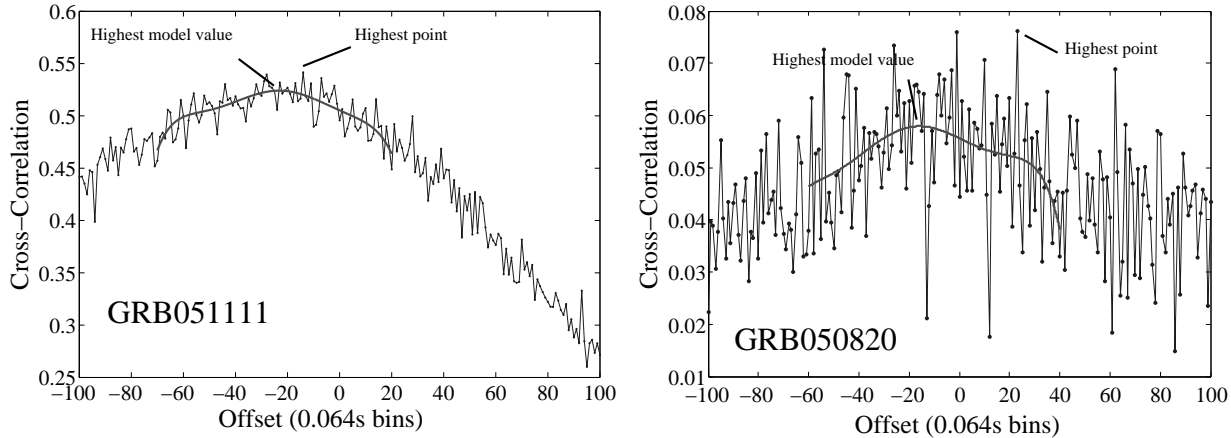


Fig. 1.— τ_{lag} calculation – Cross-Correlation versus Offset plots. The left panel is the plot for GRB051111, which is a moderately bright burst without much noise in the light curve. But we can see that although the curve is relatively smooth, the peak region is quite 'broad' that we still need an accurate fitting of the curve, especially for the central region of the curve. Had we simply taken the offset of the highest measured cross-correlation, we would have the peak at -14 bins (with τ_{lag} equal to 0.90 seconds), with this value being determined by noise in the cross correlation. Instead, we fitted a 7-order polynomial (smooth curve) and found a peak at -23.1 bins (with τ_{lag} equal to 1.48 seconds), and this model fit is avoiding most of the random noise in the cross correlation. Note, for our choice of bands, the lag will be negative in bins but expressed as positive in time. The right panel is for GRB050820, which is a noisy burst. There is much scatter in the cross-correlation versus offset plot, from which we cannot determine the position of the peak without making a fit around the peak region. In this case, the highest cross correlation is at +23 bins (corresponding to a negative lag of -1.47 seconds), with the model fit (a 7-order polynomial also) providing a more reasonable peak at -15.7 bins ($\tau_{lag} = 1.00$ seconds).

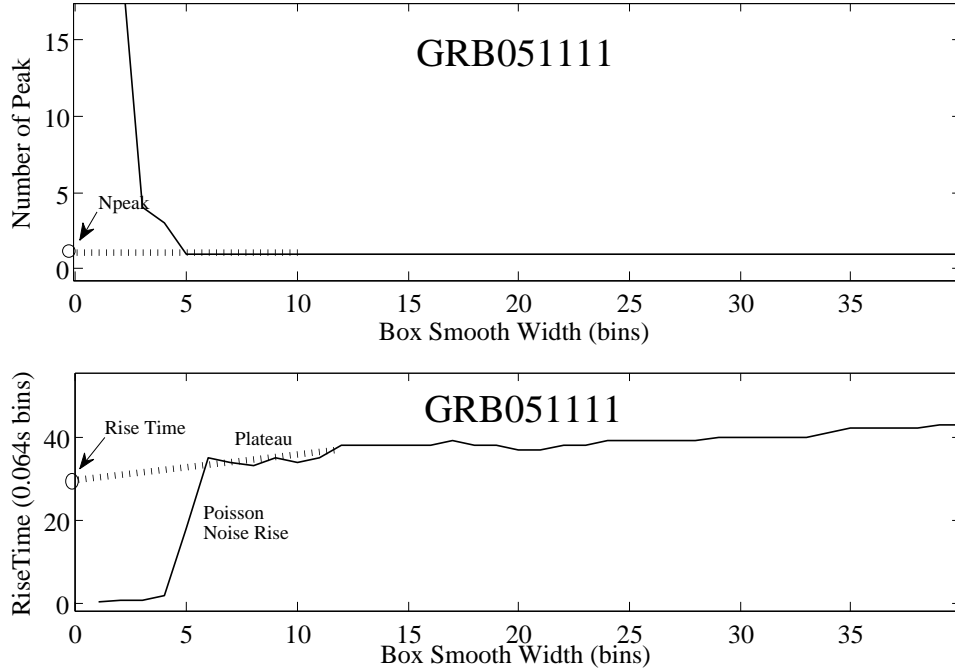


Fig. 2.— The calculation of τ_{RT} and N_{peak} . We can see an apparent 'plateau' in the lower plot, for box smoothing widths of more than 5. By simply extrapolating the plateau back to the y-axis (see dashed line), we get a minimum rise time (see circle at intercept on y-axis) which is appropriate for zero smoothing, and which is not affected by the Poisson noise.

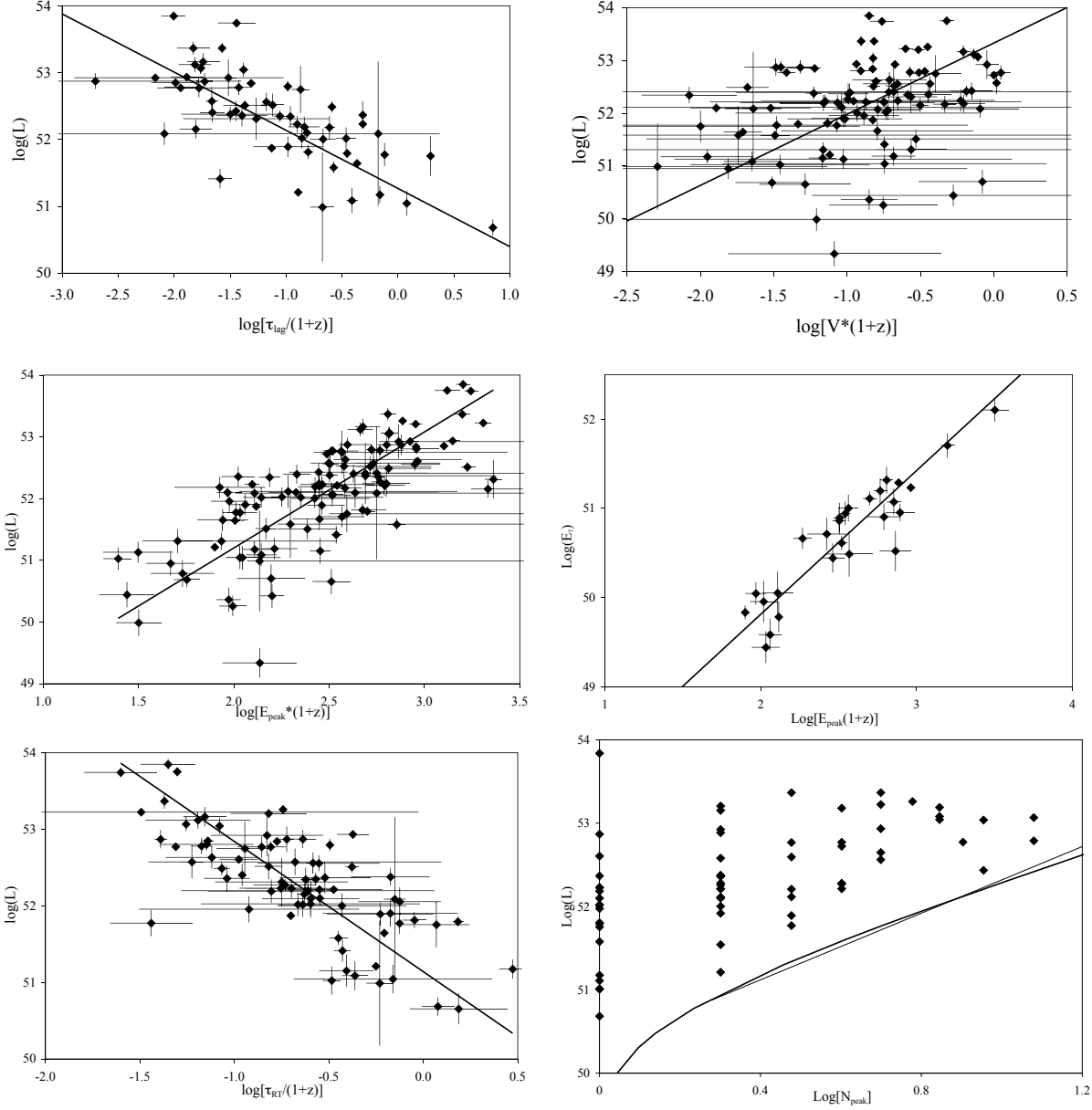


Fig. 3.— Luminosity relations for long GRBs. τ_{lag} , V , τ_{RT} and N_{peak} values are generated from light curves of the GRBs, while E_{peak} values are generated from the spectra. The $1 - \sigma$ measurement uncertainties are used as the error bar. The best fit relation of the six is the $E_{peak} - E_{\gamma}$ relation (Ghirlanda’s relation), while the most scattered one is the $V - L$ relation. However, with the restrictions on the measurements of E_{peak} (especially for Swift bursts) and jet break time, not many bursts can be included in the Ghirlanda’s relation. The $N_{peak} - L$ relation provides only a lower limit on the luminosity, but this is a strong limit never violated, for example where a 10-peak burst always has $L > 10^{52.32}$ ergs.

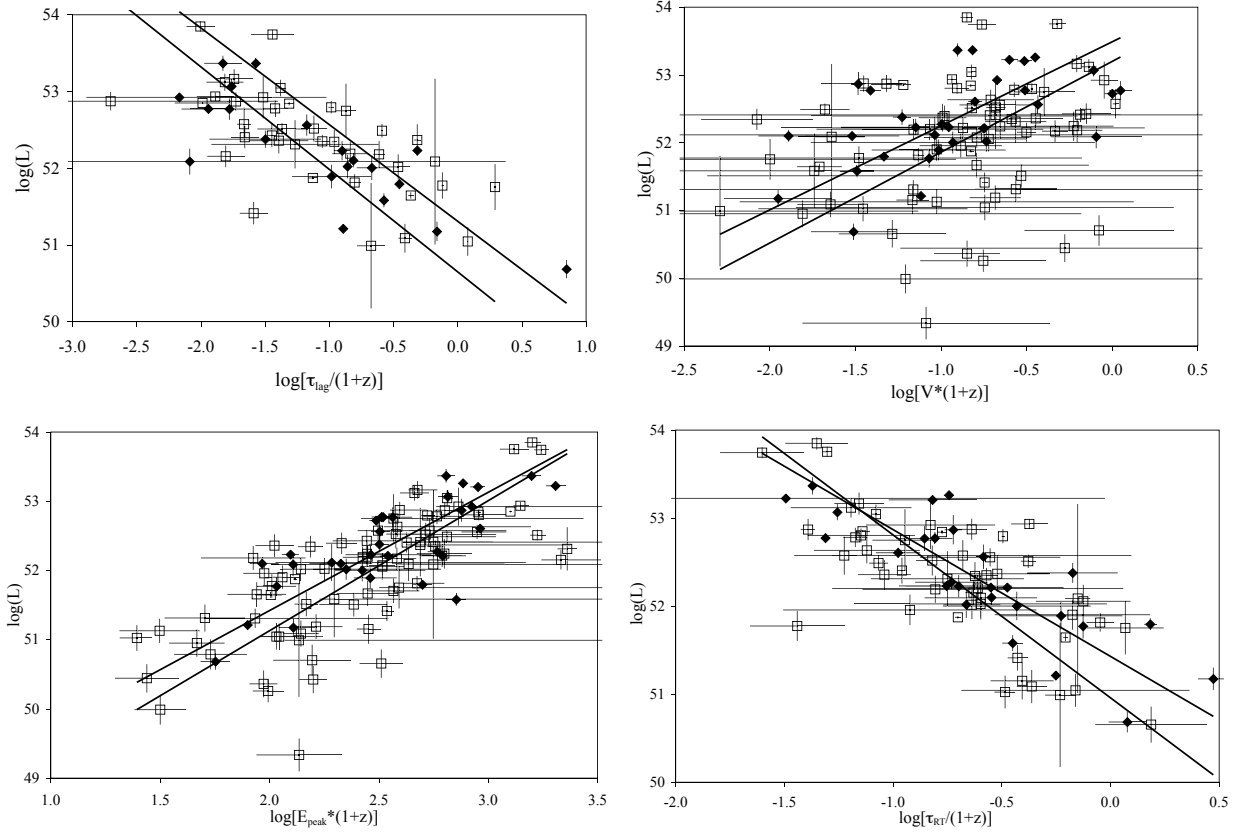


Fig. 4.— Comparison of the luminosity relations for pre-Swift and Swift bursts. The filled diamonds are for pre-Swift bursts, while the open squares are for Swift bursts. From the plot we can tell that the luminosity relations are identical between pre-Swift and Swift bursts to within the usual uncertainties. Ghirlanda’s relation is not compared because the sample of bursts with both E_{peak} and jet break time is too small.

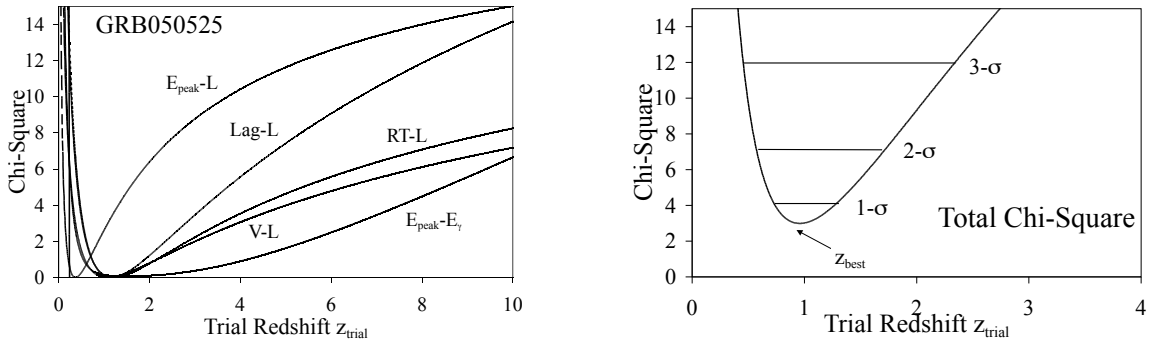


Fig. 5.— One example of the χ^2 plot in our calculation. Taking the μ_{cos} as model value and each of the μ_i as observed value, we can have the χ^2 for each of the indicators, as shown in the left panel. Each of the luminosity relations corresponding with these curves are labeled just beside the lines, and the vertical line on the left is the luminosity lower limit given by the $N_{\text{peak}} - L$ relation. We sum up all the included χ^2 s to get a total χ^2 plot, as shown in the right panel. Then the minimum χ^2 corresponds with our z_{best} , and $\chi^2 = \chi_{\text{min}}^2 + 1, 4, 9$ gives us the 1,2,3- σ range of our estimated redshifts.

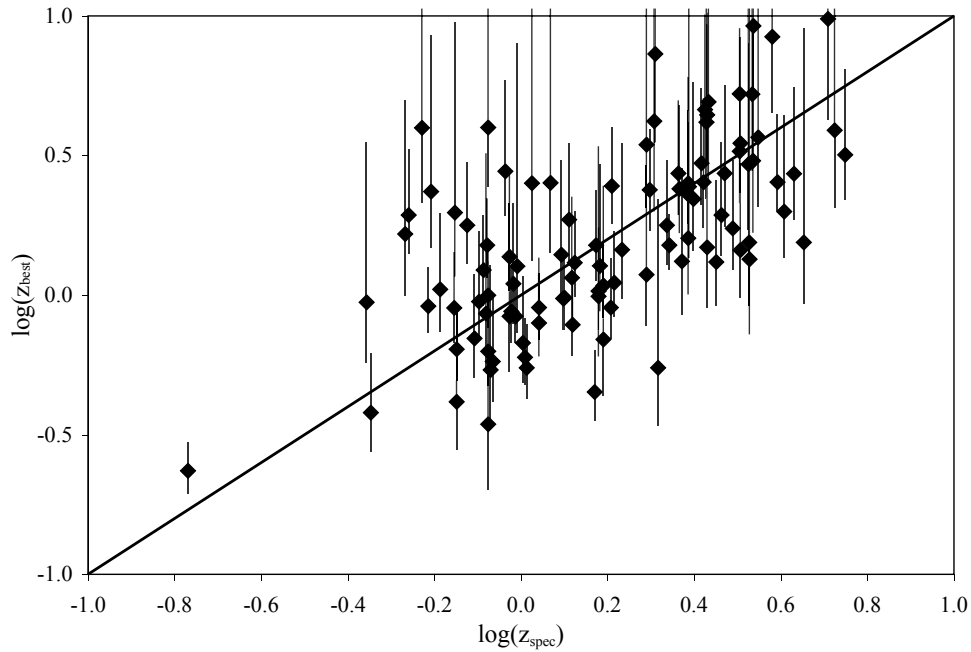


Fig. 6.— Comparison of our redshifts with spectroscopic redshifts. The diamonds are our z_{best} and the error bars gives the $1\text{-}\sigma$ redshift range. We can see that 70% of the spectroscopic redshifts fall in our $1\text{-}\sigma$ range, and our z_{best} scatter uniformly around the spectroscopic redshift (with $\langle \log(z_{best}/z_{spec}) \rangle = 0.01$). This demonstrates that our method has accurate error bars and negligible biases.

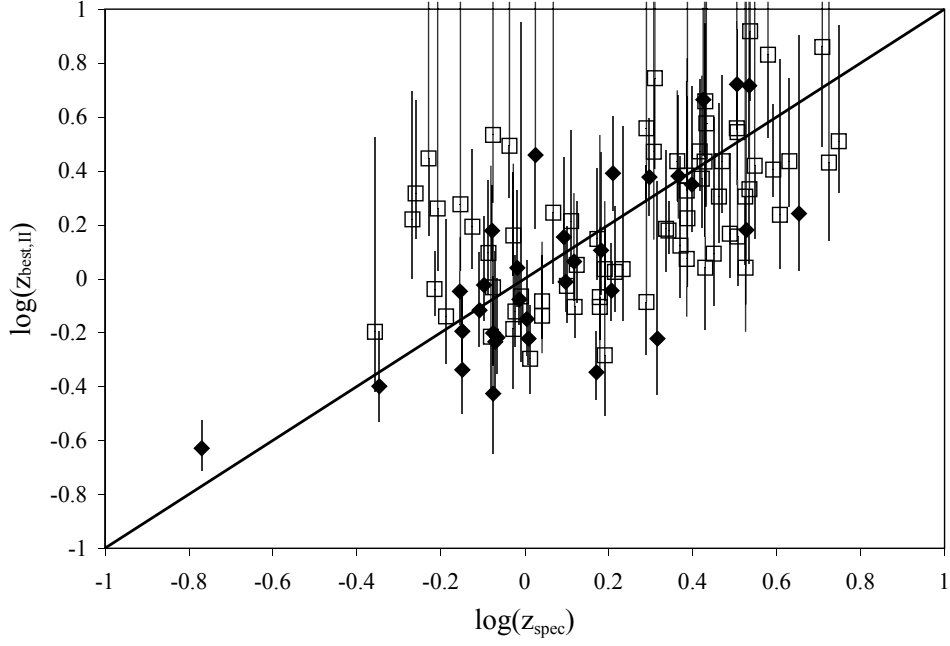


Fig. 7.— We made a comparison between our z_{best} and $z_{best,II}$. $z_{best,II}$ are the calculated redshift values when we apply *Swift* luminosity relations on pre-*Swift* data and pre-*Swift* relations on *Swift* data. The analysis on $z_{spec,II}$ and z_{spec} data shows that the average value of $\log_{10}(z_{best,II}/z_{spec})$ is -0.02, and the RMS scatter of $\log_{10}(z_{best,II}/z_{spec})$ is 0.27, both of which are equal to those of our z_{best} value within error bars. From this we see that these two sets of redshifts do not differ much from each other, which also means that the pre-*Swift* luminosity relations and *Swift* luminosity relations do not have significant difference. It also tells us that the effect of redshift involved in our calculation is negligible.